University of Genoa
Ph.D. Course in Experimental Medicine

Curriculum: **Cellular and Molecular Pathology of Age-related Diseases**

(XXXII Cycle)

Set-up of a 3D Human Trabecular Meshwork Cell *in vitro* model for the study of the pathophysiology of the aqueous humor conventional outflow pathway, through the use of oxidative and pressor stimuli and medical compounds.

Candidate: Dott.ssa Sara Tirendi *Tutor*: Prof. Nicola Traverso

Coordinator of the PhD Course: Prof.Giambattista Bonanno

A.A. 2018-2019

Summary

SUMMARY **2**

INTRODUCTION **5**

1.1 GLAUCOMA 5

1.2 EYE ANATOMY 6

1.2.1 The Cornea *8*

1.2.2 The Retina *9*

1.3 PATHWAYS THROUGH THE AQUEOUS HUMOR OUTFLOW SYSTEM 11

1.3.1 Aqueous humor functions *11*

1.3.2 Conventional or trabecular meshwork outflow pathway *11*

1.4 TRABECULAR MESHWORK 12

1.5 PRIMARY OPEN ANGLE GLAUCOMA (POAG) 14

1.5.1 POAG Pathogenesis *15*

1.6 GLAUCOMA DIAGNOSIS AND TREATMENT 18

1.7 GLAUCOMA MODEL 20

1.7.1 In vivo models *20*

1.7.2 In vitro models *22*

RESEARCH PURPOSE **25**

1ST TASK: **26**

1.1. EVALUATION OF DIFFERENT RESPONSES IN 2D- AND 3D-HTMC IN VITRO MODELS, UNDER STATIC CULTURE CONDITIONS, AFTER PROLONGED OXIDATIVE STRESS EXPOSURE. **26**

MATERIALS AND METHODS **26**

1.1.1 CELL CULTURES 26

1.1.2 EXPERIMENTAL CONDITION: PROLONGED OXIDATIVE STRESS EXPOSURE (72HRS) 27

1.1.3 CONFOCAL ANALYSIS 28

1.1.4 DCF ASSAY 28

1.1.5 MTT ASSAY 29

1.1.6 ALAMAR BLUE ASSAY 29

1.1.7 HUMAN APOPTOSIS ARRAY 29

1.1.8 QPCR ANALYSIS 30

1.1.9 WESTERN BLOT ANALYSIS 31

1.1.10 STATISTICAL ANALYSIS. 32

RESULTS 32

CONCLUSIONS **40**

1.2. EVALUATION OF DIFFERENT RESPONSES IN 3D-HTMC IN VITRO MODELS, UNDER BOTH STATIC AND DYNAMIC CULTURE CONDITIONS, AFTER PROLONGED OXIDATIVE STRESS EXPOSURE **43**

MATERIALS AND METHODS **43**

1.2.1. Cell cultures 43

1.2.2. Dynamic 3D HTMC model 43

1.2.3. Experimental condition: prolonged oxidative stress exposure (168hrs) in 3D HTMC model under static and dynamic culture conditions. 44

1.2.4. Alamar Blue Assay 44

1.2.5. qPCR analysis 44

1.2.6. Human Apoptosis Array 45

1.2.7. Western Blot Analysis 45

1.2.8. Confocal Analysis 45

1.2.9. Statistical Analysis. 45

Results 46

CONCLUSIONS **54**

2ND TASK: EFFECTS OF FLOW PRESSURE INCREASE ON 3D HTMC DYNAMIC MODEL, WHEREAS THE INCREASE IN IOP IS ONE OF THE MAIN RISK FACTORS OF GLAUCOMA. **57**

MATERIALS AND METHODS **57**

2.1. Cell Cultures 57

2.2. Experimental conditions: applying of flow pressure increase in dynamic 3D - HTMC models. 57

2.3. Alamar Blue Assay 59

2.4 Confocal Analysis 59

2.5 qPCR analysis 59

2.6 Western Blot Analysis 59

2.7 Statistical Analysis 60

Results 61

CONCLUSIONS **65**

3RD TASK: EVALUATION OF THE USEFULNESS OF THE PROPOSED IN VITRO PLATFORM TO CHECK THE EFFECTIVENESS OF TARGETED THERAPIES **67**

MATERIALS AND METHODS **67**

3.1. Cell Cultures 67

3.2. Experimental conditions 68

OS *and iTRAB® on dynamic 3D-HTMC model.* 68

increased flow pressure and iTRAB® on dynamic 3D-HTMC model. 68

3.3. DCF Assay 69

3.4. Alamar Blue Assay 69

3.5. qPCR Analysis 69

3.6. Human Apoptosis Array 69

3.7. MTT assay 69

RESULTS: EFFECTS OF ITRAB ON OS 70
3.8. *Preliminary findings on effects of iTRAB® on oxidative stress* 75

RESULTS: INCREASED PRESSURE FLOW AND *iTRAB®* ON DYNAMIC *3D-HTMC* MODEL. 76
3.9. PRELIMINARY FINDINGS ON EFFECTS OF iTRAB® ON INCREASED PRESSURE IN DYNAMIC 3D-HTMC MODEL 78

FINAL DISCUSSION 79
REFERENCES 82
PUBLICATIONS 95

Introduction

1.1 Glaucoma

The word Glaucoma derives from the greek "γλαυκός", meaning light-blue, with reference to characteristic color that is developed by opaque and edematous corneas [1]. Glaucoma represents a wide group of irreversible neuro-degenerative diseases characterized by progressive reduction of the visual field. Worldwide over 90 million people are affected by this disease, which manifests itself in a silent and painless manner but leads to progressive loss of sight [2]. Glaucoma occurs predominantly later in life even if some congenital and juvenile forms of glaucoma exsists, due to dysgenesis of the outflow system.

Up to now, since the exact pathogenesis of glaucoma is not fully understood, several risk factors, such as elevated intraocular pressure (IOP), age, family history, oxidative stress, gender, ethnicity, central corneal thickness, and myopia are associated with this disease[3–5]. However, out of these, the level of intraocular pressure seems to be related both to the optic nerve chronic damage and to the retinal ganglion cell death [6,7]. Indeed, several studies in the past, based on a large population, have confirmed that by reducing IOP, we can also reduce the glaucoma progression in patients with or w/o elevated IOP.

The collection of glaucomatous diseases is subdivided into two main subtypes: open angle glaucoma (OAG) and angle closure glaucoma (ACG) (**Figure 1**); in both optic nerve degeneration is the clinical outcome. In particular, the OAG besides being the predominant pathological form, can occur as high-pressure glaucoma (Primary Open-Angle Glaucoma POAG) and low-pressure glaucoma (Normal Tension Glaucoma NTG) [8].

However, OAG and ACG can have primary or secondary causes, based on absence or presence of other inciting factors. Indeed, secondary glaucoma can result from many other

pathologic processes, including inflammation, tumor, shock, pseudoexfoliation, and so on [3,7].

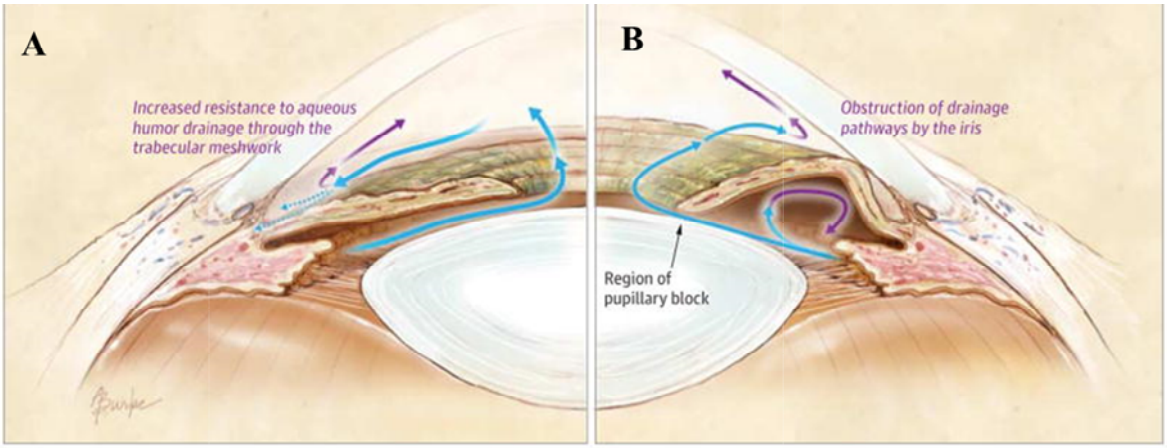

Fig.1. Representation of OAG and AGC.

A) In OAG the major site of resistance to outflow of aqueous humor (HA) is at the trabecular meshwork (TM) level. This causes an increase of intra ocular pressure inside the eye.

B) In ACG the trabecular meshwork and the uveoscleral outflow resulted blocked as a result of the iris impairment [3]

1.2 Eye Anatomy

The human eye is one of the most complex organs, and is specialized for vision. So, anatomically it can be distinguished in three layers (**Figure. 2, Panel A**):

- The **fibrous layer** consists of the cornea and the sclera. The cornea refracts and transmits the light both to the lens and the retina. In addition, it plays a protective eye role against infection and structural damage to the deeper parts. The sclera is the layer rich in collagenous fibres, elastic fibres and fibroblast which protects the eye from internal and external forces, maintaining eye shape thanks to the tendons of the oculomotor muscles. Its visible part is covered by the conjunctiva. Cornea

and sclera are connected at the limbus. The limbus (**Figure 2, B**) is the region which includes the Trabecular Meshwork (TM), a crucial tissue that, together with the Schlemm's canal, is involved in conventional outflow of aqueous humor pathway.

- The **vascular layer** of the eye is composed by the iris, the ciliary body and the choroid. The iris through the control of the pupil size, controls the amount of light which reaches the retina; the ciliary body is the site of aqueous production and controls both the power and the shape of the lens; and the choroid is a vascular layer which provides oxygen and nutrients to the inner retinal layers.
- The **neural layer** of the eye is the retina, a complex, layered structure of neurons that capture and process light.

The three transparent structures surrounded by the ocular layers are called the aqueous, the vitreous and the lens.

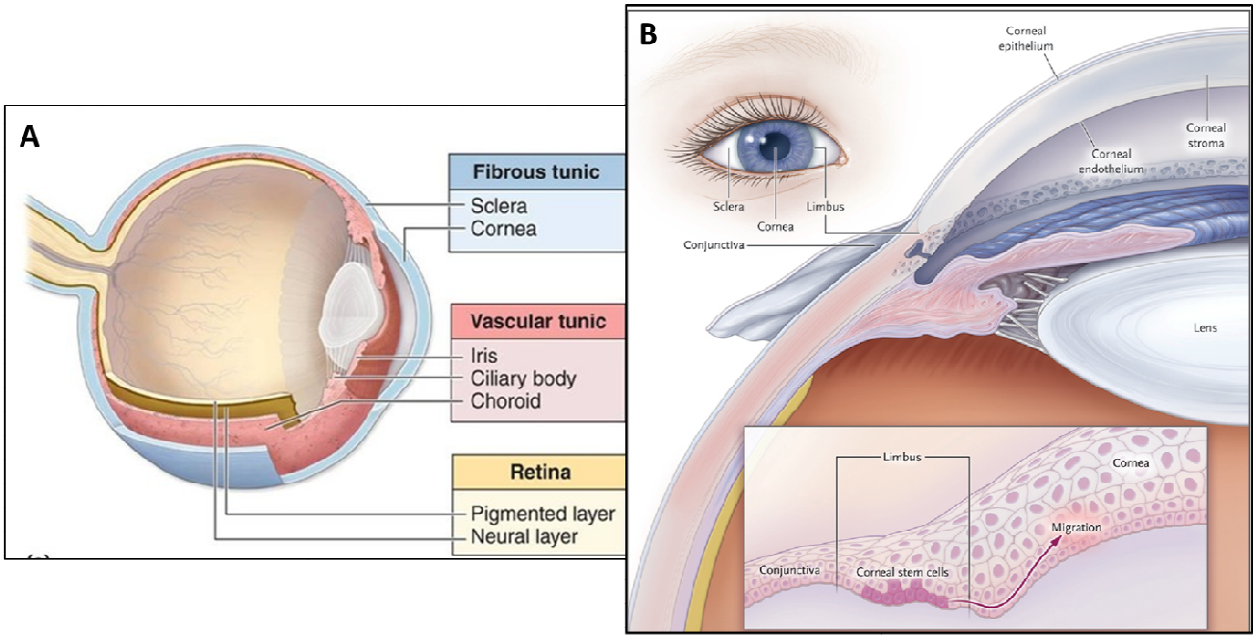

Fig.2: A) Anatomy and schematic representation of the human eye layer. B) A schematic representation of the point of union of cornea and sclera: The limbus [9].

1.2.1 The Cornea

The cornea is the most anterior part of the eye, in front of the iris and pupil. Cornea is considered the most densely innervated tissue of the body, and most of its nerves are sensory nerves, derived from the ophthalmic branch of the trigeminal nerve [10]. This tissue is avascular, indeed the branches of the anterior ciliary arteries stop at the limbus forming arcades which supply the peripheral cornea.

Five layers can be distinguished in the human cornea: the epithelium, Bowman's membrane, the lamellar stroma, Desçemet's membrane and the endothelium.

The corneal epithelium is extremely impermeable and stable due to the presence of cell junctions and it is anchored to the basal lamina. It consists of an outer lipid layer and an inner water-mucous layer and is covered by the tear film with protective functions on corneal surface from chemical, toxic or foreign body damage, microbial invasion and from smoothest out micro-irregularities. Moreover, the corneal epithelium is composed by two-three layers of superficial cells, two-three layers of wing cells and one layer of basal cells [11]. Its cells are renewed every 7–10 days from a pluripotent stem cell population, which resides in the palisades of Vogt at the corneoscleral limbus [12]. However, previous studies has also identified an oligo potent stem cell population from mice and pig epithelium, suggesting that there are niche for corneal stem cells besides the limbus [13] (**Figure.2, Panel B**).

The Bowman's layer is separated from epithelium by stroma. Bowman's layer is anacellular zone composed by collagen fibrils network which is responsible for the cornea mechanical strength and for its transparency [14].

The stromal collagen fibrils are surrounded by proteoglycans with an important structural function in hydration regulation. The predominant stroma cell type are Keratocytes and they play a role in maintaining the stroma organization.

The corneal endothelium consists of a single layer of five-seven-sided cuboidal cells with little or no self-renewing potential. They secrete the Descemet's membrane that separates the endothelium from the stroma. This elastic membrane is composed of an anterior layer with a banded appearance and a posterior layer with an amorphous texture [15].

The endothelium possesses intracellular and membrane-bound ion transport systems and the resulting osmotic gradient produces a net fluid flux from the stroma to the aqueous which is essential for the clarity and transparency of the cornea (i.e. deturgescence) [16].

1.2.2 The Retina

The retina is the tissue that lines the inner surface of the eye, surrounding the vitreous cavity. During embryogenesis, the vertebral retina develops from the optic cup. The latter is formed by invagination of the optic vesicle, which is an outgrowth of the embryonic forebrain. The inner wall of the optic cup becomes the neural retina while the outer wall becomes the retinal pigment epithelium (RPE) [17].

The neural retina consists of six major classes of neurons: photoreceptors, bipolar cells, horizontal cells, amacrine cells and ganglion cells and the Müllerian glia (**Figure.3**).

The eyes of most vertebrates contain two types of photoreceptors: rods and cones. In humans, rods are approximately 20 times more abundant than cones [18]. The photoreceptors are responsible for conversion of light into an electrical signal (phototransduction), therefore the membranes of the outer segment discs contain pigments. Cones are responsible for colour vision and have pigments with absorption peaks in the blue, green or yellow parts of the spectrum (rods pigments have an absorption peak in the blue-green part of the spectrum). In humans, about 50% of the cones are located in the central 30% of the visual field, roughly corresponding with the macula.

Histologically, the macula has several layers of ganglion cells unlike peripheral retina which has the ganglion cell layer thick only one-cell. The excavation near the center of the

macula is called the fovea and it is responsible for sharp central vision. Fovea contains the largest concentration of cones in fact, the visual acuity is highest in this region [18].

The RPE is a monolayer of cuboidal epithelial cells intercalated between the photoreceptors and the choriocapillaris.

At the apical side, the cells of the RPE form long microvilli that are extended between the outer segments of rod photoreceptors and its cytoplasm contains numerous pigment (i.e. melanin, lipofuscin) granules. The RPE main features include the maintenance of photoreceptor function (phagocytosis of photoreceptor wastes, regeneration and synthesis of pigments), retinal adhesion, storage and metabolism of vitamin A, the production of growth factors necessary for nearby tissues and wound healing after injury or surgery [19,20]. In addition, the RPE plays an important role in the blood–retinal barrier (BRB) function. Retinal function depends on several factors, including the region of the retina being illuminated, the wavelength and the intensity of the light stimulus and the state of light adaptation.

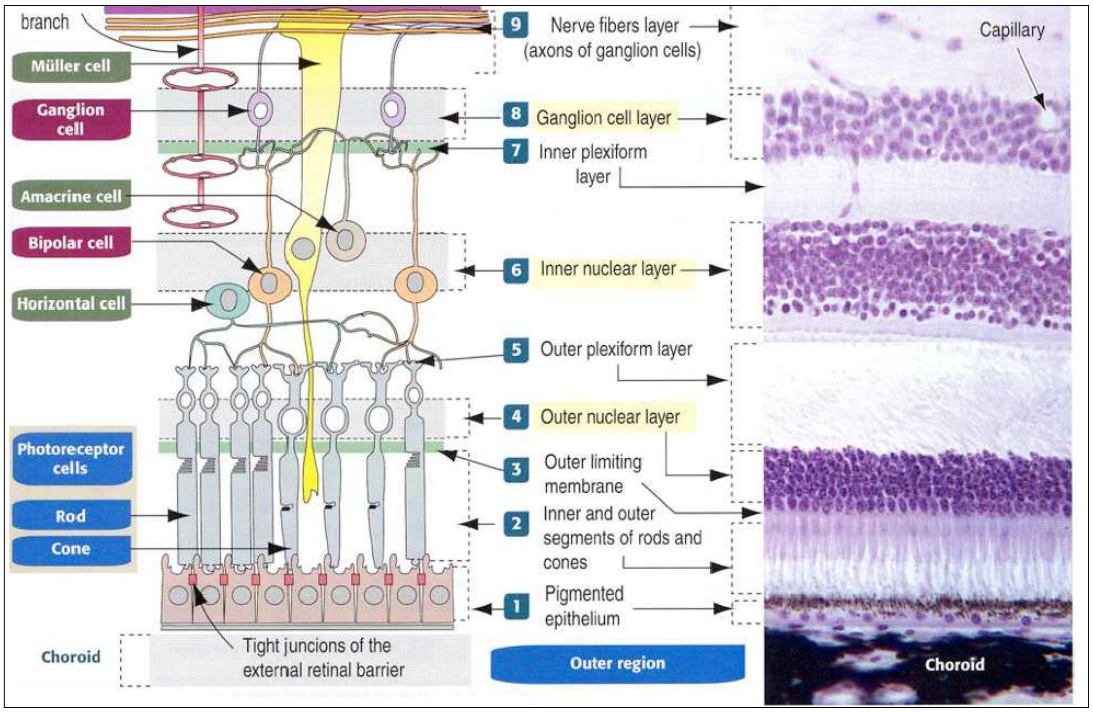

Fig.3: The layers of neural retina [21].

1.3 Pathways through the Aqueous humor outflow system

1.3.1 Aqueous humor functions

Aqueous humor (AH) is a clear fluid produced by the ciliary body (CB) epithelium consisting both of a pigmented ciliary epithelial (PE) cell layer and a non-pigmented ciliary epithelial (NPE) cell layer facing the stroma and the posterior chamber of the eye, respectively. After, the AH flows from anterior chamber to episcleral veins passing through TM (**Figure.4**).

AH, wetting the anterior chamber of the eye, provides nutrients and removes waste products. In physiological conditions, the balance in aqueous inflow and outflow rate, regulates the IOP in order to maintain the shape and related refractive properties of the eye [21].

1.3.2 Conventional or trabecular meshwork outflow pathway

The AH returns to the venous system thought *conventional or trabecular meshwork outflow pathway* (**Figure.4**). The TM represents the proximal portion of the aqueous outflow system and it has been estimated that this tissue drains ~ 70–90% of AH. TM is divided into distinct regions: the uveal meshwork, the corneoscleral meshwork, and the Juxtacanalicular region.This latter, is located between the last trabecular lamellae and Schlemm's canal (SC) inner wall endothelium. Therefore, AH crosses the SC inner wall endothelium to enter SC either through pores or through transcanalicular conduits arising from SC endothelium. Moreover, AH can drains out through the uveoscleral pathway which includes the ciliary body and other structures [22,23]

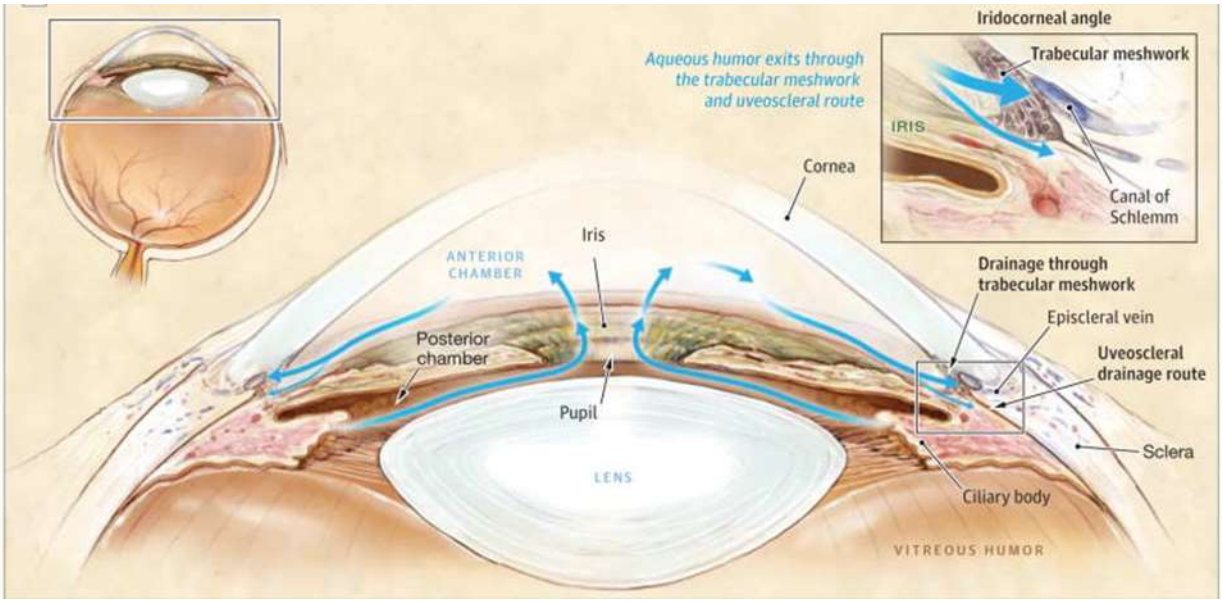

Fig.4: Anatomy of healthy eye and aqueous humor drainage pathways [3]

1.4 Trabecular meshwork

The trabecular meshwork (TM) is an essential, and perhaps the most important, tissue which together with a complex organ system dependent on several tissue components, working in unison to maintain a homeostatic IOP.

TM structure consists of the inner uveal trabecular meshwork (UTM), the deeper corneoscleral trabecular meshwork (CTM), and the Juxtacanalicular region (JCT) or cribriform region. In addition, exists a fourth region considered “non-filtering” but contains of a TM stem cell populations, below the Schwalbe's line, named the “insert” region of the TM.

The UTM is characterized by 1-3 layers of trabecular beams or lamellae, while the CTM by 8–15 trabecular layers, which are thicker than those of the UTM and originate from the scleral spur [24]. Each trabecular beam consists in a core of collagen (types I and III) and elastin fibers covered by flat cells that rest on a basal lamina rich in collagen type IV and laminin [25–27]. The beams rearrange in several layers forming the porous filter-like

structure and changes depending on TM region. The porous size of the uveal and corneoscleral meshworks range in size from 25–75 μm in the proximal regions to 2–15 μm in the deeper layers of the corneoscleral meshwork. Moreover, in the outer region (JCT region) the fenestrations became more tight with a porosity that ranges between 30 and 50% [28,29].

Among the main TM tissue functions, the filtration and the resistance to outflow resistance regulation, are recognized. Nevertheless, the differences in cells morphology and function, TM cells have a common embryological origin, the neural crest [30].

The AH drains through the inner TM and thanks to the macrophage-like activity of UTM and CTM cells, is clarified by cellular debris derived from shed pigmented epithelia or waste materials before reaching the JCT region. Therefore, a defective macrophage activity, could be responsible for secondary form of glaucoma [31]. Then, the tight fenestrations of the outer TM region (JCT) together with the inner SC cells, work together physically and functionally to generate outflow resistance, in order to restrict flow of aqueous humor into the lumen of SC and onto the systemic venous system [28]. Indeed, both smooth-muscle like and fibroblastic qualities of JCT cells, respectively, allows them to regulate the AH outflow contracting the JCT region and SC wall and to regenerate ECM proteins every 48 hrs [32,33].

Moreover, the TM cells, as endothelia, produce large quantities of antithrombotic substances like heparin sulfate and tissue-plasminogen activator (tPA) [34], participate in antigen presentation and inflammation pathway, producing major histocompatibility proteins and a wide array of inflammatory cytokines, respectively [35,36]. This latter feature results important after laser trabeculoplasty because the rapid secretion of IL-1α and TNFα in response to the injury, stimulates extracellular matrix turnover and debris phagocytosis [37].

1.5 Primary Open Angle Glaucoma (POAG)

POAG is a chronic, progressive, and irreversible multifactorial chronic disease, which affects a large proportion of the population over the age of 40 years. Glaucoma clinical outcome leads to blindness through a neurodegeneration process which extends beyond the retina and optic nerve into the visual pathway [38].

Currently, POAG etiology remains obscure, probably due to the heterogeneous and complex nature of the disease, both on a clinical and on a molecular level. In this regard, several research work have identified some of risk factors and genetic causes such as aging, elevated IOP (≥ 22 mm Hg), race and a positive family history, involved in glaucoma onset [39,40].

Indeed, it has been estimated that the prevalence of glaucoma increases sharply with age, probably because its onset may be associated with other age-related diseases such as macular degeneration, vascular diseases, obstructive sleep apnea, and so on. Moreover, the state of frailty related to aging, depends on the accumulation of health deficits (i.e. hypertension, hypotension, diabetes, migraine, obstructive sleep apnea syndrome, cataracts, glaucoma) and results in a higher risk for accelerated physical and cognitive decline, disability and death [41,42].

It seems that also race impacts on prevalence of POAG due to differences in exposure to geographic, social, behavioral and environmental factors. In particular, the black American population is more predisposed to POAG than whites.

In addition, several epidemiological evidence demonstrated that a positive family history of POAG increases its insorgence risk about 2.1 times. Therefore, the development and integration of many genetic approaches were used to identify genome regions that are associated with both a specific phenotype and specific genetic variants. The first approach

to identify chromosomal locations for Mendelian forms of POAG was the Family-based genetic linkage analysis which led to the identification of many POAG-associated loci and, less often, specific causative genes. So, genetic mutations for POAG have been identified in three genes: myocilin (MYOC), optineurin (OPTN), and TANK binding kinase 1 (TBK1). In addition, the differential expression analysis of mRNA and proteins have added to our understanding of human genetic disorders [43–45].

1.5.1 POAG Pathogenesis

Back in 1854, Albrecht Von Graefe described the mainly clinical POAG features by the triad including IOP, optic disc excavation and laminar lacunation and specific field loss [46].

However, from the last century is known that oxidative stress (OS), inflammation, excitotoxicity, vascular impairment and hypoxia, glial dysfunction and altered axonal transport are the most pathogenic mechanisms recognized [47–50]. In particular, OS appears to play a pivotal role in TM damage in term of a decrease of mitochondrial respiratory activity, an inflammatory cytokine release, an impairment of extracellular matrix (ECM) components and its turnover, a cellular senescence promotion and consequent a loss of its cellularity, and so on [51,52].

Therefore, an impairment of TM functions leads to outflow resistance and IOP increase, in a region known as the juxtacanalicular tissue (JCT) or cribriform region [53].

As known, TM together with the JCT, the endothelial lining of Schlemm's canal, the collecting channels and the aqueous veins, represent the major drainage structure for aqueous humor (AH) i.e. the *conventional* or *trabecular outflow pathways* [25]. In addition, some fraction of AH flow out from the eyes through an *unconventional* or *uveoscleral outflow route* [22].

So, in a physiological condition, the fluid flows rate across the *trabecular outflow pathways* equals the rate of AH produced by the ciliary body but this balance is subject to alteration with age and POAG. Therefore, an "extra" resistance in AH outflow due to cellular dysfunction, including the TM, results in elevated IOP [54]. Morphological and biochemical alterations of TM common to several patients with POAG have been observed including the loss of cells, increased accumulation of extracellular matrix proteins (ECM), changes in the cytoskeleton, cellular senescence, and the process of subclinical inflammation. In particular, the TM extracellular matrix (ECM) and its turnover play a significant role in modulating AH outflow [54–56]. As known, in physiological conditions the ECM contains collagens, laminins, elastin, fibronectin, fibrillins, proteoglycans, matricellular proteins, etc. However, several previous *in vitro* studies highlighted that the differences in ECM composition of glaucomatous patients, in terms of a decrease in hyaluronic acid and an increase in chondroitin sulfate, correlated with flow resistance. Moreover, also Grow Factors (i.e. TGFβ-2) and gene expression (i.e. SPARC, MYOC, MMPs) are being modulated [57–61] determining an overexpression of various ECM components and IOP increase [55,62].

Moreover, with regard to RGCs apoptosis, two theories were proposed as final outcome of glaucomatous cascade: the mechanical and vascular theories.

The mechanical theory, as the name implies, supports that the mechanical action of the IOP is directly responsible both of optic nerve head compression and the axoplasmic transport cessation, thus resulting in apoptosis of RGCs and their axons [63]. However, the limits of such hypothesis are related to the lack of this clinical sign in some types of glaucoma (i.e. NTG).

The vascular theory, instead, explains that the RGCs death is caused by insufficient blood flow of the optic nerve head due to several issue such as IOP, high blood pressure,

vasospasm and so on [5,63]. Indeed, also diseases like obstructive sleep apnea (OSA) and diabetes mellitus type 2 (DM2), are linked to vascular failure [64,65] and POAG.

1.6 Glaucoma diagnosis and treatment

Since glaucoma has no symptoms in its early stage, it has not been possible yet to identify specific molecular and physiological disease markers [66]. Early diagnosis, with regular and complete eye exams, is important to protecting the vision from damage caused by glaucoma. Five common tests are crucial to detect glaucoma: tonometry, ophthalmoscopy, perimetry, gonioscopy and pachimetry.

Tonometry measures the pressure within the eye. The range for normal pressure is 12-22 mm Hg and, usually, more glaucoma cases are diagnosed with pressure exceeding 20mm because eye pressure depends on the individual. After a preliminary examination, follows ophthalmoscopy exam (fundus examination) or optical coherence tomography (OCT), because the fundus is the only location where vasculature can be visualized. The fundus is the anterior face of the eye opposite to the lens and includes: retina, optic nerve, macula and fovea (**Figure.5**). The glaucoma pathologic feature includes the optic nerve head "excavated" or "cupped" which results as reduced fovea region vascularization. Furthermore, viewing the fundus is a great way to undestand the patient's overall vasculature. For example, the ophthalmoscopic exam, allowed to discover pathological processes otherwise invisible: endocarditis, disseminated candidemia, CMV in an HIV infected patient, and being able to find both diabetes and hypertension.

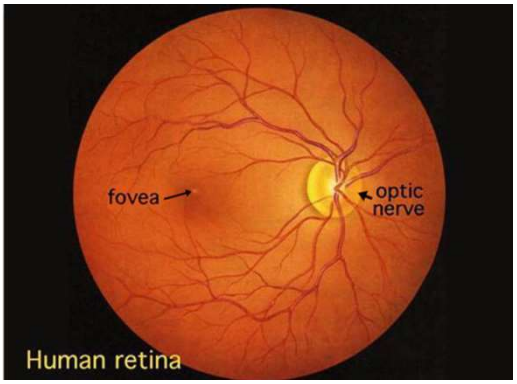

Fig.5: A view of the healthy human retina seen though an ophthalmoscope. [67]

When disease is diagnosed, the exam of visual field, (perimetry exam) and the gonioscopy constitute an important step to understand the map of complete field of vision. The perimetry exam helps to clarify whether the vision has been affected by glaucoma, when a moving light passes peripheral (or side) vision. Gonioscopy exam helps determine wheter the irido-corneal angle is open and wide or narrow and closed. During the exam eye drops are used to numb the eye. The angle closed and blocked it is a possible sign of angle-closure, acute glaucoma; but the angle wide or open is a possible sign of open-angle, chronic glaucoma.

Finally, the pachimetry exam is simple, painless and measure the thickness of the cornea and it could be help the glaucoma diagnosis because corneal thickness has the potential to influence eye pressure state [68–70].

As known, up today the IOP is the only modifiable risk of glaucoma, therefore, the first-line treatment is represented by ocular hypotensive drops with or w/o antioxidants (polyphenols) preparation as adjuvants, to slow the disease progression. However, also the surgery approach (trabeculoplasty) is used to reduce the eye pressure [71].

In this regard, several studies have demonstrated that the polyphenols, whose are product of plant metabolism, are capable of defending cells against free-radicals. Indeed, are recommended for the several pathological states such as cancer, diabetes, osteoporosis, cardiovascular and neurodegenerative disease. As reported by Graft et al (2005) and Arts&Hollman (2005), a diet rich in polyphenols is able to counter the inflammatory state in order to reduce the risk of chronic disease [72,73]. Another further study showed that the eye drops containing Perilla Frutescens with certain flavonoids, catechins and fatty acids concentrations, have a protective role on TM from oxidative stress damage [74].

Moreover, several studies have been focused on RGCs degeneration arrest in glaucoma. So, it has been reported the neuroprotective effect of the citidin difosfocolina-5-(citicoline) in addition to the hypotensive therapy [75–77].

1.7 Glaucoma model

1.7.1 In vivo models

Animal models are widely used in several research field, in particular to study multifactorial diseases [78]. Given the evidence that glaucoma is linked with the IOP increase, animal induced-models are common used to mimic the effects of IOP elevation on RGCs [79]. However, they do not describe the early stage of glaucomatous cascade.

Many animals have been used including monkeys, dogs, mouse, rats, zebrafish, rabbits, sheep, cows, birds, even though, the most representative of human ocular anatomy are non-human primates (i.e. monkeys), but due to both ethical and economic reasons, their use is very limited. In order to mimic the IOP increase, several techniques have been developed such as laser photocoagulation of the perilimbal region, autologous fixed red blood cell injection or microbeads injection into the anterior chamber, episcleral vein obstruction, hypertonic saline injection into the episcleral veins, and so on [80–82].

1. **Laser photocoagulation of the perilimbal region**. Several studies have used laser photocoagulation which induced the IOP elevations lead to an increase of resistance of outflow pathways, through the angle closure and the SC destruction. Gasterland and Kupfer (1974) [83] developed an experimental monkey model that became the standard for laser-induced glaucoma. In this experiment they applied circumferential argon laser photocoagulation to the TM in each monkey eyes for 4-times. The IOP range was between 24 and 50 mmHg and remain elevated for 30 days. This method induce ocular inflammation in anterior chamber and irreversible mydriasis. Moreover, the variability of IOP magnitude and duration makes this approach not amenable [84,85]. Unlike the monkeys, rat and mice model are more easy to maintain in laboratory. Indeed, Levkovitch- Verbin (2002) [86] induced experimentally glaucoma in Wistar rats using laser photocoagulation to TM or episcleral veins through the external limbus. Laser

photocoagulation has led to closure both of intrabecular spaces and the outflow conventional pathway. In addition, after 3 weeks of induced elevated IOP , showed RGC loss and axonal damage of the optic nerve. But, even in this model, there was limitations: the pigmentation of the TM, in rats, lead to a different effects to IOP increase and this treatment induced ocular inflammation and corneal opacity.

2. **Microbeads or autologous fixed red blood cell injected into the anterior chamber**

   To overcame the disadvantages of laser photocoagulation the microbeads or autologous fixed RBC were injected into the anterior chamber of the eye in primates, mice, rats, and rabbits [87–89] to induce IOP trough the inhibition of aqueous outflow [84].

   This approach avoids intraocular inflammation but it is not amenable because the microbeads are not preserved in anterior chamber angle after injection [90].

3. **Episcleral Vein Obstruction.**

   Shareef et al. (1995) [91] developed a rat model of glaucoma, that includes an episcleral vein cauterization which lead to an increase of IOP. This method is less invasive than laser photocoagulation and induces no complications in the anterior chamber [92]. Because of its efficacy and accessibility, the majority of the structural and functional studies in experimental glaucoma have used this method. This technique, as reported by Shareef et al. (1995), does not create complications in the eye anterior chamber [93]. However, the adverse outcome affect intraocular inflammation and ocular surface damage.

4. **Hypertonic saline injection into the episcleral veins.**

   Episcleral vein saline injection result an increase in the resistance of acqueous outflow channels. Kipfer-Kauer et al. (2010) [94] in C57BL/6 mice have injected with 1.5M hypertonic saline into a limbal vein for inducing chronic IOP elevation. Unfortunately, the induction technique is relative difficulty and it requires

considerable training and experience. Then, the duration of IOP elevation is shortly and sequential injections are required to produce IOP changes over time [95].

Some physiopathological mechanisms of glaucoma have been explained by animal models, however, the lack of species specific together with the non-standardized experimental conditions make impossible understand all molecular implications to develop new drugs and pharmacological interventions [84].

1.7.2 In vitro models

Experimental system *in vitro* are useful to standardize experimental conditions enabling easier manipulation of specific variables, which contribute to degenerative changes of glaucoma [96]. In this regard the clinical practice and the research studies on glaucoma, have not provided yet a real correlation between the first marks of ocular degenerations and the evolution of neurodegenerative implications which lead to irreversible blindness [97].

Indeed, several in *vitro* TM model help to clarify the mechanism involved in glaucoma disease and to provide new insights into the molecular mechanisms of disease progression [57] [82].

Therefore, it is important to make species- specific study by using human specific models. 3D human cultures represent the starter point for reliable in *vitro* model because they preserve the physiological relevance in vivo conditions [98], unlike 2D cultures [99].

In a standard procedure, 3D cultures are cultured in a static environment, which in time lead to a loss of several cellular functions. Now, it is possible recreate a more complex 3D system capable to reflect the in vivo conditions of cells and, also, the injection of chemical gradients required (i.e. nutrients and oxygen) by using of a peristaltic pump. In particular,

in in *vitro* model the used of bioreactor technologies, thanks to a “milli-fluidic” system, aim to improve the 3D cultures quality by providing, in a constant flow rate, to a continuous medium support without exposing cells to a high shear force [100,101]. In literature, there are examples of pathological models of heart, lung, intestinal, kidney, endocrine, bone-muscle and neurological diseases [101]. These in-vitro models are, in fact, more relevant to human physiology because they permit the studying of cell-crosstalk and the building of complex in-vitro models as well as allowing further investigation of a tissue or an organ and that of their interaction, avoiding the use of animals and following EU Commission directives. However, in order to provide an alternative to standard method, through the use of dynamic conditions, cells can condition their habitat and interact with others, secreting cytokines, and mimicking a real live situation, thanks to the flow of medium between the different tissues. This aspect increases cell survival and proliferation, allowing, at the same time, the cross-talk between different tissues cultivated in different chambers (the so-called inter-organ communication). Moreover, this approach permits the study of not only the effect of the drug on the target tissue but also the side-effects on the related organs which are in communication due to the medium flow.

Furthermore, in some in *vitro* models the elevated of hydrostatic pressure (EHP) have been used in several context such as cancer [102,103], hypertension and platelet aggregation [104], and cartilage and chondrocyte response [105]. Then, as glaucoma is strongly associated with IOP increased, EHP has been used to mimic ocular hypertension on TM cells [106,107]. Following the use of bioreactor technologies, the pressure elevation, according to the circadian rhythm, was induced by LivePa, a device able to increase by the 10% the inner pressure inside the culture chamber, thanks to a plunger fitted on it.

Nevertheless, it is good to keep in mind that *in vitro* models do not mimic the intricate glaucomatous pathology and do not replace the animal models, but could help to clarify the

mechanism of this disease and to answer to some important question in a faster and cheaper way [81].

Research purpose

The aim of my research work was focused on three different tasks.

1. Comparison of the biological differences of different HTMC cell in vitro models to verify which one could best mimic the TM impairment after prolonged oxidative stress exposure. In particular, in this task has been subdivided into two steps:
    - Evaluation of different responces in 2D- and 3D-HTMC in vitro models, under static culture conditions, after prolonged oxidative stress exposure.
    - Evaluation of different responces in 3D-HTMC in vitro models, under both static and dynamic culture conditions, after prolonged oxidative stress exposure.
2. Effects of flow pressure increase on 3D HTMC dynamic model, whereas the increase in IOP is one of the main risk factors of glaucoma.

3. Evaluation if the proposed in vitro platform can be considered as an useful tool to check the effectiveness of targeted therapies through the modulation of the biomarker levels identified. For this purpose, the effects of a concentrated mixture of polyphenols (ITRAB®) was analysed in 3D-dynamic HTMC model submitted to prolonged oxidative and pressure stimuli.

1st Task:

1.1. Evaluation of different responses in 2D- and 3D-HTMC in vitro models, under static culture conditions, after prolonged oxidative stress exposure.

MATERIALS AND METHODS

1.1.1 Cell cultures

Human trabecular meshwork cells (HTMC) and Trabecular Meshwork Growth Medium (TMGM) were from Cell APPLICATION INC. (San Diego, CA, USA). According to consensus recommendations reported by Keller et al. [108], Cell APPLICATION laboratory gave the official report on the evidence that HTMC cells, made available by their Company, express several markers related to a trabecular phenotype, since the HTMC resulted responsive to Dexametasone treatment by increased protein level expression of fibronectin, α-smooth muscle actin, myocilin and the cross-linked actin networks (CLANs) (see: https://www.cellapplications.com/human-trabecular-meshwork-cells-htmc).

Standard HTMC cultures were performed as monolayers and grown in TMGM at 37◦C in a humidified atmosphere containing 5% CO_2, according to the manufacturer's indications and were sub-cultured by TripLE™ Express (Invitrogen Life Technologies) treatment when the original flask was approximately 75% confluent.

3D cultures were performed by embedding HTMC into Corning® Matrigel® Matrix (Corning Life Sciences, Tewksbury, MA USA). Briefly, a suspension of 500,000 HTMCs was slightly centrifuged for 5 min at 90 rcf, and after removing the supernatant, the cell pellet was gently resuspended in 200 µl of undiluted Matrigel™ at 4°C. The embedded

HTMCs were then gently transferred by pipette into culture chambers (1.9 cm^2 growth area/dish) and the culture medium was added (1ml/dish) after 15 min, which is the necessary time for the Matrigel to reach its gelling state. Then each culture chamber was incubated under standard culture conditions.

2D and 3D-HTMC were seeded at 4 x $10^4/cm^2$ and 2.5 x $10^5/cm^3$ cells, respectively, in Primo® TC Flask 25 cm^2, and 96-wells plate (Euroclone®, Milano Italy), in BD-FalconTM cultures Slides (BD Biosciences Europe, Erembodegem, Belgium) and in Millipore TC-Plate 24-wells (Merck S.p.a., Merck KGaA, Darmstadt, Germany),

After seeding both 2D and 3D HTMC cultures were maintained in low and high glucose DMEM (1:1 mix) , 2mM L-glutamine, 0.5% gentamicin and 100µg/ml streptomycin, w/o Fetal Bovine Serum (FBS) [109], in order to reduce any FBS interference on cellular proliferation.

At the end of the experimental time 2D and 3D HTMCs were harvested by TripLE™ Express and from 3D Corning Cell Recovery (Corning Life Sciences B.V., Amsterdam, NL), respectively.

All cell cultures were found to be mycoplasma-free during regular checks with the Reagent Set Mycoplasma Euroclone (Euroclone® Milan, Italy).

1.1.2 Experimental condition: Prolonged oxidative stress exposure (72hrs) in 2D-HTMC vs. 3D- HTMC static models.

Prolonged oxidative stress was induced in 2D- and 3D-HTMC up to 72 hrs, by daily exposure for 2 hrs to 500µM H_2O_2, with 22-hour recovery phases in between, according to Poehlmann et al., 2013 [110]. The H_2O_2 concentration was selected on the basis of previous experiments to identify a dose that resulted subtoxic, with a MTT viability index > 75% versus untreated cultures (data not shown).

1.1.3 Confocal analysis

At each selected check point time untreated and treated 2D- and 3D-HTMC were set in 4% paraformaldehyde and permeabilized with 0.3% Triton X-100 (Sigma Aldrich®, Milan, Italy). Nuclei were stained with To-Pro^{TM} -3 Iodide 642/641(Thermofisher Scientific Inc., Monza, Italy), actin cytoskeleton was visualized using Phalloidin Alexa Fluor 488 (Cell Signaling Technology, Danvers, USA). Fluorescence signals were captured at 60X magnification, by Leica TSC SP microscope (Leica Microsystem, Wetzlar, Germany) and elaborated by Fiji-ImageJ software, an open-source platform for biological-image analysis. Signals from different fluorescent probes were taken in sequential scan settings (3D reconstruction images).

1.1.4 DCF Assay

The monitoring of ROS production was performed by using the dichlorofluorescein (DCF) assay. 2D- and 3D-HTMC cultures were exposed to non-fluorescent 2',7'-dichlorodihydrofluorescein diacetate (H2DCFDA, ThermoFisher Scientific Inc.), that freely permeates the plasma membrane and is reduced to the highly fluorescent 2',7'-dichlorofluorescein [111]. Experiments were performed in 96-well plates, and each condition analysed 6 times. Cells were seeded in 2D culture medium or in 3D Matrigel as already described at 10,000 cells/well the day before. After removing the culture medium, HTMCs were briefly rinsed with Hank's balanced salt solution (HBSS) with calcium and magnesium and incubated with 10 μM H2DCFDA in HBSS at 37°C in 5% CO_2 for 45 min. Then the H2DCFDA solution was removed and cultures were washed with HBSS and challenged with 500μM H_2O_2 in order to evaluate the ROS production over time in both culture models. DCF emission was determined at 2hr, on a fluorescent plate reader, at excitation and emission wavelengths of 485 and 520 nm, respectively. The fluorescence

intensity was extrapolated after subtracting the blank (medium plus DFC for 2Ds and Matrigel plus medium plus DCF for 3Ds) and was expressed as percentage of relative fluorescence unit of treated vs untreated HTMC cultures.

1.1.5 MTT Assay

At the end of each experimental treatment, the cell viability in terms of mitochondria functionality was assessed in 2D and 3D models by MTT assay [112]. The optical densities (OD) of the dissolved formazan crystals was determined spectrophotometrically at 570 nm. The quantification of cell viability was obtained by comparing the optical density of the extracts, and relative cell viability was calculated for each tissue as Arbitral Unit (AU), extrapolated by Optical Density (OD) of the samples.

1.1.6 Alamar Blue Assay

The 2D- and 3D-HTMC healthy state, in terms of their metabolic activity, was measured by Alamar Blue™ (InVitrogen Life Technology) assay daily, during the last 4 hrs before the end of the 22 hrs of recovery time, by adding 10% Alamar Blue™ directly in culture medium. The assay was carried out according to the manufacturer's instructions. At each check point time, the resazurin reduction was extrapolated spectrophotometrically by monitoring absorbance at 570 and 630 nm wavelength. The results were expressed as AU extrapolated by OD of each sample.

1.1.7 Human Apoptosis Array

Apoptosis was investigated by the semi-quantitative detection of 43 human apoptotic proteins, on customized Human Apoptosis Array C1 chip (RayBio®; Norcross, GA) (**Table 1**). Briefly, after cell lysis each sample was incubated with antibody array membrane ON at 4°C. The day after, each membrane, after repeated washings with the Wash Buffer I and II (provided with the kit), was incubated with biotinylated antibody cocktail for 2 hrs at RT.

Then, after washings with abovementioned Wash Buffers, membranes were incubated with HRP-Streptovidin for 2 hrs at RT. After further washings, each membrane was incubated with detection buffer and the chemioluminescence was detected on radiographic plate. The intensity of protein array signals was analysed using a BIORAD Geldoc 2000 and each protein spot was normalized against Positive Control Spots printed on each membrane.

The data analysis was conducted following the Protocol directions of Human Apoptosis Array C1. The raw numerical densitometry data were subtracted from background (Negative Control signals) and normalized to the Positive Control signals. To determine the relative protein expression on different arrays, relating to untreated and treated samples, the algorithm according to Human Apoptosis Array C1 protocol was used.

	A	B	C	D	E	F	G	H	I	J	K	L	M	N
1	POS	POS	NEG	NEG	Blank	Blank	bad	bax	Bcl2	Bcl2-w	BID	BIM	Caspase3	Caspase8
2														
3	CD40	CD40L	cIAP2	CytoC	DR6	Fas	FasL	Blank	Hsp27	Hsp60	Hsp70	HTRA2	IGF1	IGF2
4														
5	IGFBP1	IGFBP2	IGFBP3	IGFBP4	IGFBP5	IGFBP6	IGF-1R	Livin	P21	P27	P53	SMAC	Survivn	TNF RI
6														
7	TNF RII	TNFα	TNFβ	TRAIL R1	TRAIL R2	TRAIL R3	TRAIL R4	XIAP	Blank	Blank	NEG	NEG	POS	POS
8														

Table 1. The mini map of Human Apoptosis Array C1 (according to RayBio® manufacturer manual)

1.1.8 qPCR analysis

After the cells were treated as mentioned above, the expression profile of selected genes was obtained by qPCR analysis. Total RNA was extracted using the RNeasy Micro Kit (Qiagen, Milan, Italy) according to the manufacturer's instructions. Quality and quantity of RNA was analysed using a NanoDrop spectrophotometer (Nanodrop Technologies, Wilmington, DE, USA). The cDNA (150 ng per sample) was synthesized by using SuperScript™ III First Strand Synthesis System (ThermoFisher Scientific, Milan, Italy). Each PCR reaction was performed in 10 µl containing: 5× HOT FIREPol® EvaGreen®

qPCR Mix Plus (Solis BioDyne, Tartu, Estonia), 0.2 μM of each primers and 1 ng of synthesized cDNA. All samples were analysed in triplicate. The following thermal conditions were used: initial denaturation/hot start for 15 min, followed by 45 cycles with denaturation at 95° C for 15 s, annealing and elongation at 60° C for 60 s. The fluorescence was measured at the end of each elongation step. The next step was a slow heating (1° C/ s) of the amplified product from 55° C to 92° C in order to generate a melting temperature curve. Values were normalized to ubiquitin (reference gene) mRNA expression. All primers (**Table 2**), were designed using the Beacon Designer 7.0 software (Premier Biosoft International, Palo Alto CA, USA) and obtained from TibMolBiol (Genova, Italy). Data analyses were obtained using the DNA Engine Opticon® 3 Real-Time Detection System Software program (3.03 version) and, in order to calculate the relative gene expression compared to an untreated (control) calibrator sample, the comparative threshold [113]. was used within the Gene Expression Analysis for iCycler iQ Real Time Detection System software (Bio-Rad) [114] . Data are means ± S.D. of at least three independent experiments performed in triplicate.

GENE	GenBank	Forward	Reverse	Size (bp)
IL-1alpha	NM_000575.4	CAATCTGTGTCTCTGAGTATC	TCAACCGTCTCTTCTTCA	112
IL-1beta	NM_000576.2	TGATGGCTTATTACAGTGGCAATG	GTAGTGGTGGTCGGAGATTCG	140
IL-6	NM_001318095.1	CAGATTTGAGAGTAGTGAGGAAC	CGCAGAATGAGATGAGTTGTC	195
Ubiquitin C	NM_021009.7	ATTTGGGTCGCAGTTCTTG	TGCCTTGACATTCTCGATGGT	50

Table 2. Primer sequences used for real time quantitative polymerase chain reaction analysis.

1.1.9 Western Blot Analysis

Cell lysates were collected using RIPA buffer (Sigma Aldrich) plus protease inhibitor cocktail (Complete Tablets, Roche Diagnostic GmbH, Mannheim Germany) and sonicated until solubilized. 25mg of proteins were resolved in Ani kD^{TM} mini precast gel (Bio-Rad Laboratories, Inc., Hercules, CA, USA) in SDS-PAGE Running Buffer and transferred

onto PVDF membrane (Thermo Scientific, Rockford, USA) and probed with primary antibodies against rabbit, phospho-NF-kB p65, Ser 536 (Cell Signaling Technology,) and mouse GAPDH (Santa Cruz Biotechnology, Santa Cruz, CA, USA) followed by incubation with HRP-conjugated secondary antibodies (NA9340V and NA931V, against rabbit and mouse primary antibodies, respectively, Amersham Life Science, Milano, Italy). The proteins were detected by Western Bright^{TM} ECL (Advansta, CA, USA), exposed to film and analysed using a BIORAD Geldoc 2000. The data presented were calculated after normalization with GAPDH. Densitometrical data obtained from Quantity One software (Bio-Rad) were applied for statistical analysis and normalized against the housekeeping GAPDH. The results were expressed as fold vs untreated cultures, respectively.

1.1.10 Statistical Analysis.

Reported data are expressed as mean ± Standard Deviation (SD) and results were analyzed using two-way analysis of ANOVA for single comparison or two-way analysis of ANOVA variance followed by Bonferroni posttest for multiple comparisons. GraphPad Prism for Windows- version 5.03 and GraphPad Software, Inc., La Jolla, CA, USA) was used. Statistically significant differences were set at $p<0.001$; $p<0.01$; $p<0.05$.

Results

Confocal analysis

Spatial organization of 2D- and 3D-HTMC cultures was analysed by confocal microscopy at the end of the experimental conditions, by cell imaging reconstruction. The merged images of untreated and H_2O_2-treated HTMC cultures did not show any visible changes both in F-actin and in the nuclei structures. However, from a qualitative point of view, 2D-HTMCs showed a reduction of cell-to-cell interaction compared to the 3D model, in which cells showed an oblong morphology and better-ordered distribution in the matrix with a

close resemblance to the in vivo physiological cell shape and an abundance of natural fibrous tissues. (**Figure .1**).

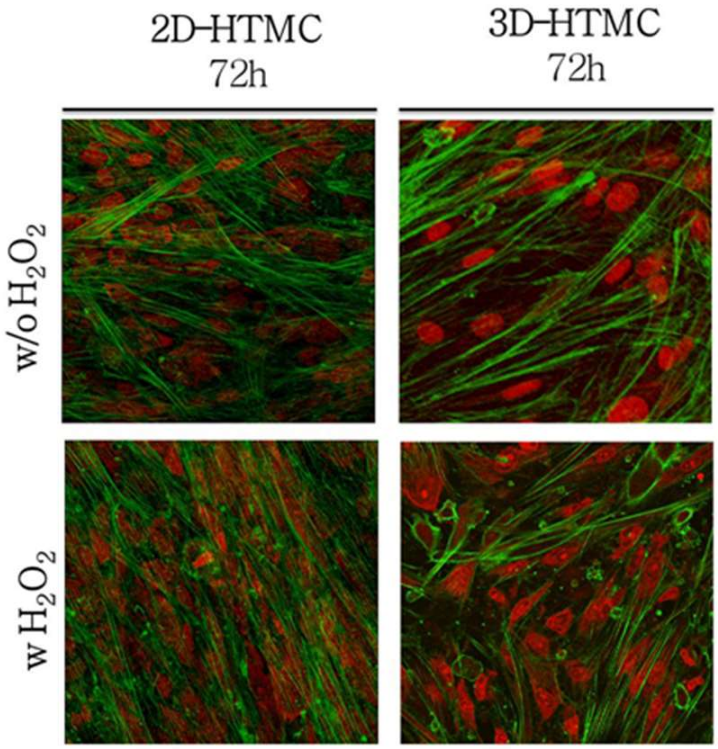

Fig.1: **Confocal analysis**. Confocal microscopy analyses of nucleus and cytoskeletal markers were performed on untreated and H_2O_2-treated 2D- and 3D HTMC cells after 72 hrs of experimental procedures. Representative images are related to immunoreactivity for To-Pro^{TM} and Phalloidin, as nuclear and cytoskeleton markers, respectively. Merged images showed cytoskeleton plus Nucleus. Fluorescence signals were captured at 60x magnification.

DCF assay

The fluorometric DCF assay was performed in order to evaluate the ability of hydrogen peroxide to induce ROS production in the 2D- and 3D-HTMC cultures. The effect of hydrogen peroxide was investigated, either keeping it or not keeping it in HTMC culture medium, beyond the two hours. In both HTMC models the ROS production was therefore quantified at 2 hrs (**Figure 2**). A different ROS production between 2D- and 3D- HTMCs over time was already observed after 2h of H_2O_2 exposure, in fact, the HTMCs cultured in 3D increased their intracellular ROS production by about 142%, compared to 2D-HTMC cultures.

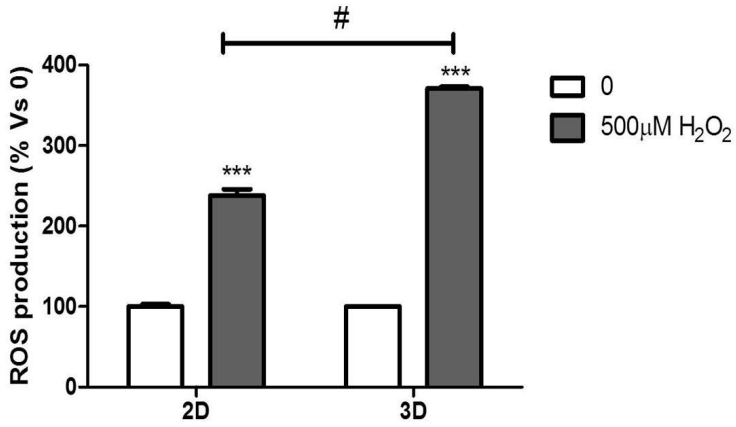

Fig.2: DCF assay. DCF assay were performed on untreated and H_2O_2-treated 2D- and 3D HTMC cells after 2 hrs of experimental procedures. Data are expressed as % of untreated HTMC and represent the mean ± SD of 3 independent experiments. ***p <0.001 vs respective untreated cultures and #p<0.001 vs 500µM H_2O_2 treated HTMC (Two-way ANOVA followed by Bonferroni's test).

Mitochondrial respiratory functionality

MTT assay was carried out as a 'gold standard' to evaluate cell viability by reference to the mitochondrial compartment functionality during chronic stress exposure (**Figure. 3, a**). After 24 hrs of experimental treatment, the viability index of H_2O_2-treated HTMC revealed an impairment in both culture models, although it was slightly more marked in 3D- than in 2D-cultures. However, during the following experimental time of exposure to oxidative stress, the mitochondrial functionality resulted restored in both 2D- and 3D-HTMC models, probably indicating an adptive response to H_2O_2.

Alamar Blue Assay

The effects of chronic 500µM H_2O_2 exposure on 2D-and 3D-HTMC were measured at each check point time up to 72 hrs, by Alamar Blue assay (**Figure. 3, b**). 2D HTMC exposed to chronic stress reflected the general trend of untreated cultures, with a decrease of resorufin reduction at the end of the experimental treatment. Conversely, untreated 3D HTMC cultures showed a constant increase of metabolic activities and even during 500µM

H_2O_2 chronic treatment. Overall, at all time points, treated 3D HTMCs evidenced a significant increase of their metabolic state as opposed to control cultures. This increment decreased slightly after 72 hrs of 500 µM H_2O_2 treatment, whilst remaining higher than untreated cells.

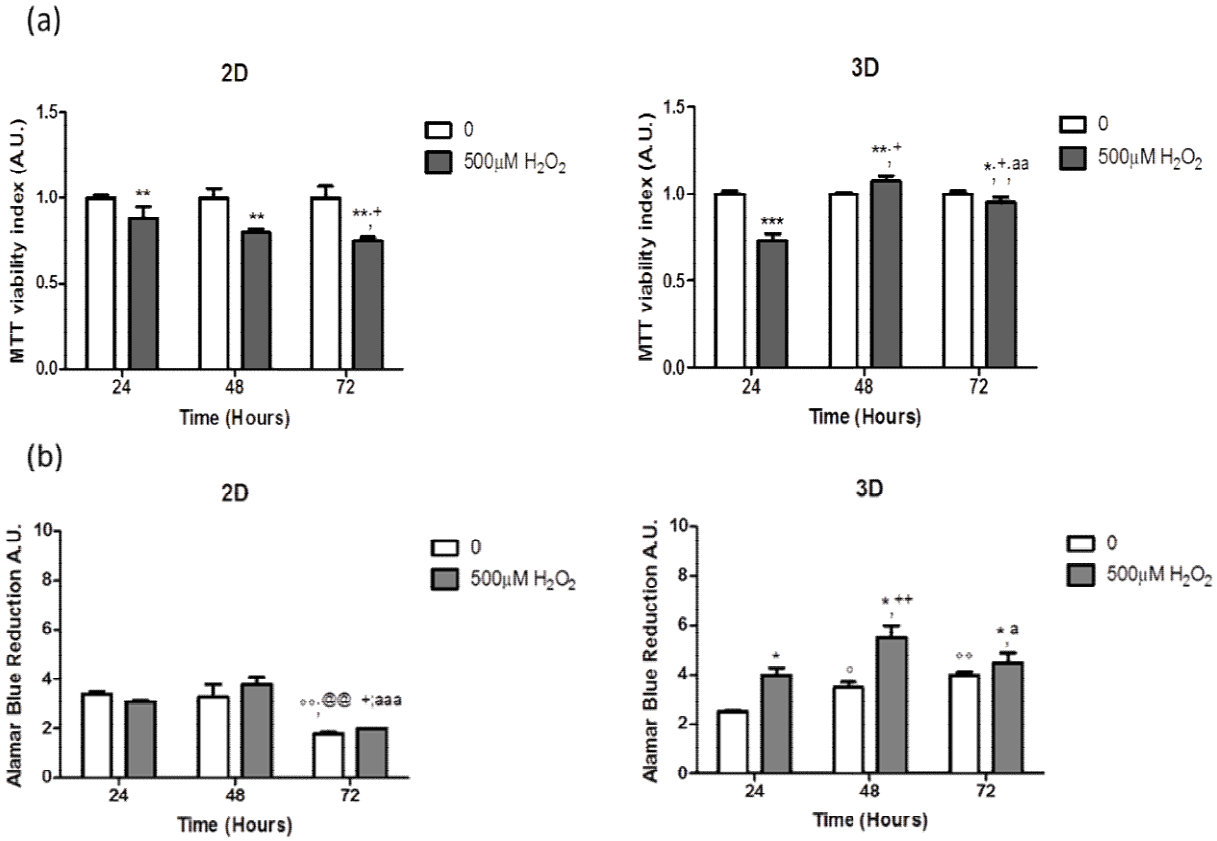

Figure 3. Effects of chronic H_2O_2 treatment on HTMC metabolic activity. (a) Mitochondrial respiratory functionality. MTT assay was performed in 2D- and 3D-HTMC exposed to H_2O_2 (500µM) for 24, 48 and 72 hrs. **(b)** Metabolic state of untreated and H_2O_2 treated 2D and 3D HTMC cultures, during experimental treatments, was evaluated by Alamar blue assay. Data are expressed as A.U. of MTT test and of resazurin reduction of each HTMC cultures, and represent the mean ± S.D of 3 separated experiments, in triplicate.
*p <0.05 treated vs respective untreated cultures; °°p<0.01;°p<0.05, untreated 48 and 72 hrs vs untreated HTMCs 24 hrs; @@p<0.01 untreated 72 hrs vs untreated HTMCs 48 hrs; +p<0.01 treated 48 and 72 hrs vs treated HTMCs 24 hrs; aaap<0.001 aap<0.01; ap<0.05, treated 72 hrs vs treated HTMCs 48 hrs. (Two-way ANOVA followed by Bonferroni posttest).

Apoptosis Array

Pro- and Anti- apoptotic protein levels were analysed by Human Antibody Array C1 (RayBio® C-Series) using 43 different antibodies (**Figure. 4**). The array patterns highlighted the differences between the 2D- and 3D-HTMC model, in apoptosis ignition. In particular, 3D-HTMCs showed a high throughput profiling in response to the hydrogen peroxide, compared to 2D.

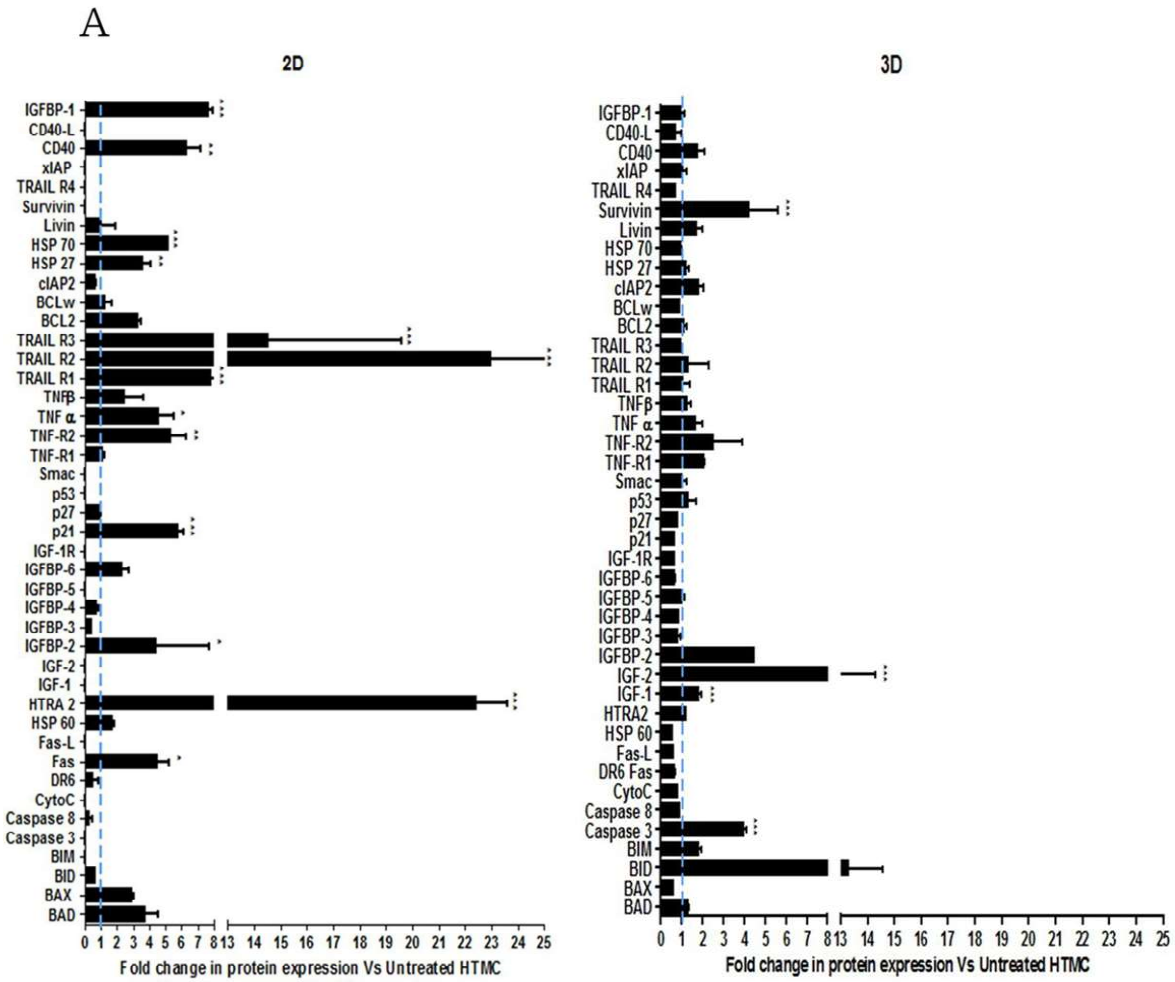

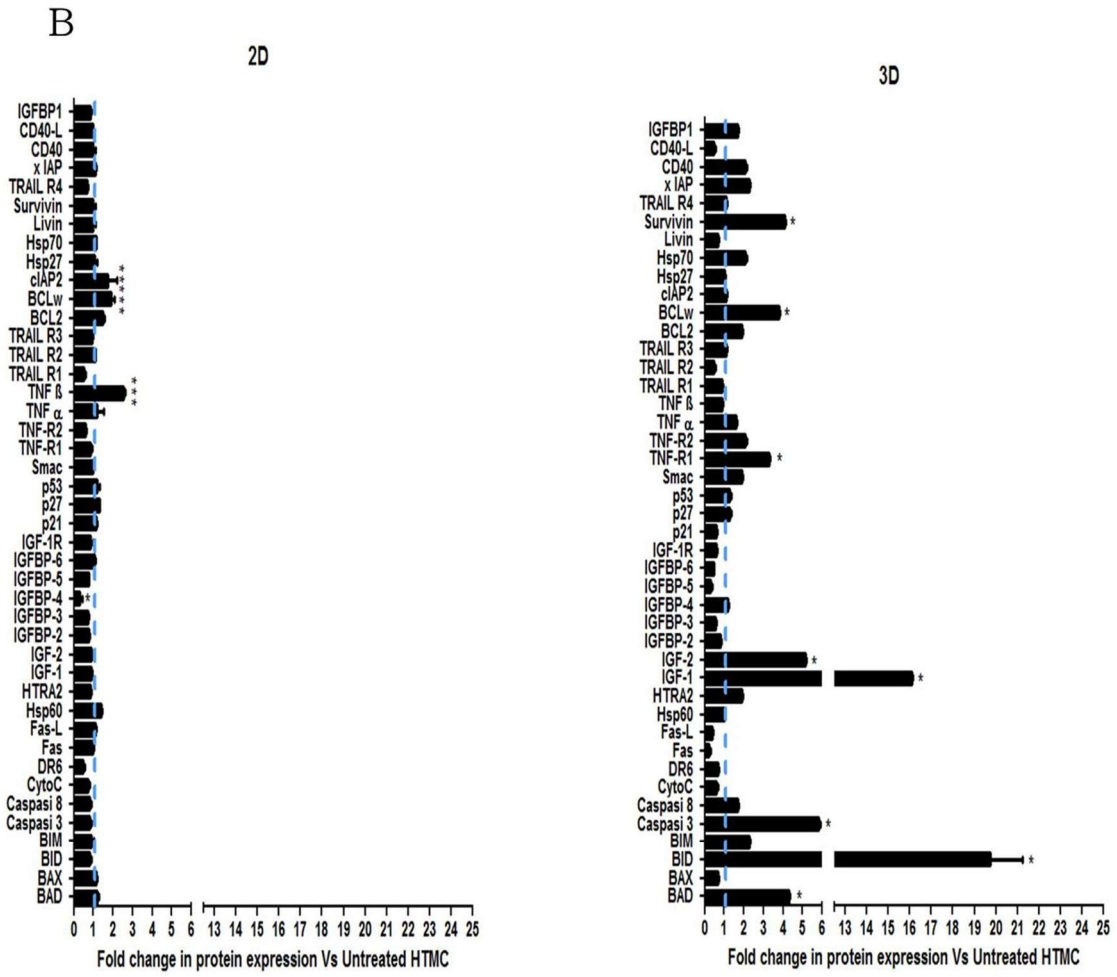

Figure 4. **Apoptosis Array**. Analysis of anti- apoptotic and pro- apoptotic protein levels in 2D- and 3D-HTMC were performed after 48 (panel A) and 72h panel B) of 500µM H_2O_2, by Human Antibody Array C1 (RayBio® C-series).The light blue dotted line represents the protein level of untreated HTMC for each of the 43 proteins examined. For each time point twelve individual models were arrayed (six 2D-HTMC plus six 3D-HTMC) and per experiment the intensity of Positive Control Spot was used to normalize signal responses for comparison of results across multiple arrays. ***p<0.001;**p<0.01; *p<0.05; vs. respective untreated cultures (One-way ANOVA followed by Bonferroni posttest).

qPCR analysis

The trigger of a pro inflammatory response in 2D- and 3D-HTMCs after **48** and **72 hrs** exposure to OS, was analysed in terms of gene expression levels of IL-1β, IL-1α and IL6 by qPCR (**Figure. 5, A**). At 48 hrs, untreated 2D HTMCs showed a lower levels of basal gene expression of all cytokines compared to HTMCs cultured in 3D conditions according to Regier et al., [115]. Moreover, at this time point, only treated 3D-HTMCs revealed a slight, but significant increase of IL1α level.

Conversely, at 72 hrs treated 2D-HTMCs showed a marked increase of IL1α of about 15 fold compared to untreated 2D-cultures, while in 3D-HTMCs an increase of IL1α, IL1β and IL6 of about 3, 2 and 1.5 fold respectively, was observed compared to the untreated 3D-HTMCs.

Western Blot Analysis

The level of NF-kB transactivation was detected by a specific kit containing antibodies against both NF-kB p65 and the phospho-NF-kB p65 subunit to check the inflammatory / antiapoptotic response activation.

2D- and 3D-HTMCs were treated for 24-48-72 hrs as mentioned above and the NF-kB activation was analysed in terms of the ratio between the levels of phospho-NF-kB p65/ NF-kB p65 (Figure 4B). Phospho-NF-kB p65 protein content was up-regulated by H_2O_2 treatment (**Figure. 5E**) only in 3D-HTMCs ($p<0.001$) when compared to both the untreated culture models and the treated 2D-models.

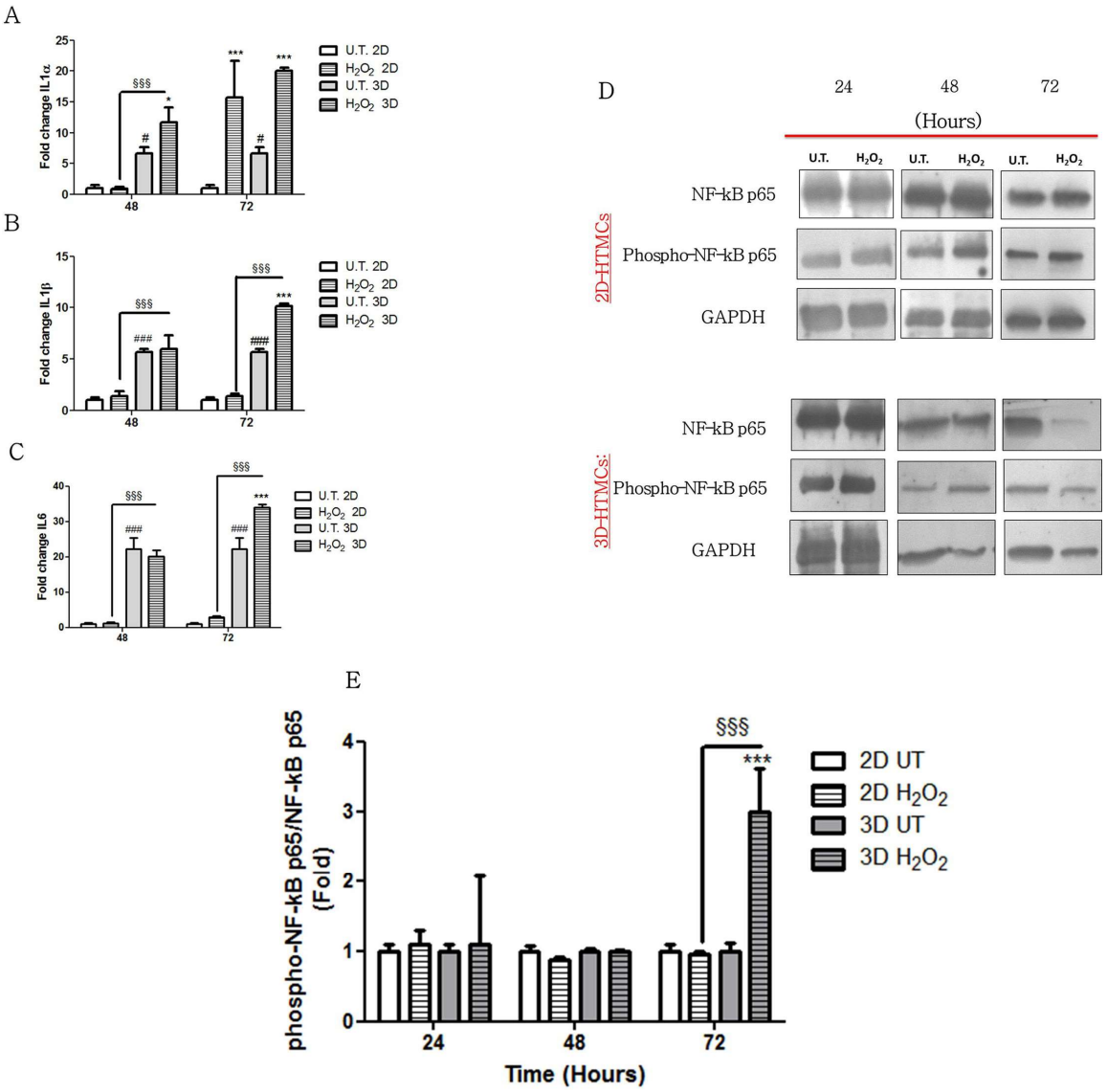

Figure 5. Induction of pro inflammatory factors by chronic H_2O_2 treatment. Quantitative PCR gene expression analysis of 2D- and 3D-HTMCs subjected to 500μM H_2O_2 for 48 h and 72 h. IL-1α(A), IL-1β (B), and IL-6 (C) gene levels. Data are expressed as fold-increase relative to the 2D and 3D control cultures at the same end-point and normalized to Ubiquitin housekeeping gene expression. Each bar represents the mean±S.D. of three independent experiments performed in triplicate. **(D)** Representative immunoblot showing NF-kB (p65) and p-NF-kB (p65) protein levels of untreated (U.T.) and treated HTMC (H_2O_2) whole protein lysates at indicated time points. GAPDH was used as an internal control for equal protein loading on the gel. **(E)** NF-kBp65 activation was evaluated in HTMC cells subjected to chronic treatment with H_2O_2 for 24, 48 and 72 hrs. The analysis was performed by immunoblotting and the bars represent the ratio of phosfoNF-kBp65/NF-kBp65, and are expressed as fold vs. untreated HTMC cultures. Data represent the mean ± S.D. of 3 independent experiments.

***p <0.001, * p <0.05 treated 3D-HTMCs vs. untreated 3D-HTMCs cells; ### p<0.001, # p <0.05 untreated 3D-HTMC vs. untreated 2D-HTMC cells; §§§p<0.001 treated 3D-HTMC vs. treated 2D-HTMC cells (Two-way ANOVA followed by Bonferroni posttests).

Conclusions

Nowadays, cell cultures are used in biomedical research, tissue engineering, regenerative medicine and industrial practices. Two-dimensional 2D cell cultures are the most popular, but is increasingly gaining ground the three-dimensional (3D) cultures with a more realistic biochemical and biomechanical microenvironments [116].

As known, in *in vivo* microenvironment all cells are surrounded by ECM and by other cells, however the 2D cell cultures due to the support accession, do not mimic the natural environment of cells [117] [118]. This was demonstrated by confocal analysis which highlighted that only HTMC embedded in Matrigel® allowed the development of the complex architecture in terms of dimension and cell-to-cell contact. Indeed, the 2D HTMC showed a more confused pattern with less definition of both F-actin and nuclear shape due to the cells flattening typical of a bi-dimensional culture condition (**Figure 1**).

Moreover, the cellular ROS production after 2hrs of H_2O_2 exposure was evaluated by DCF assay in order to demonstrate that the matrix used for 3D cultures did not interfere with HTMCs biological response. In our previous work [119], we analysed the cellular ROS production after H_2O_2 over time and it has already been demonstrated that 2 hr exposure time was sufficient to promote the intracellular ROS production without difference in terms of cytotoxicity exerted by H_2O_2.

Therefore, the 3D model shown a higher sensitivity to OS compared to standard 2D cultures because their spatial architecture maintained a more physiological setup (**Figure 2**).

Regarding the maintainance of cell health state, we observed that the flattening of 2D cell culture influences many cellular processes including cell proliferation, apoptosis, gene and protein expression, while the 3D culture thanks to the interactions between cell to cell and

cell to ECM preserves the cell functions found in vivo [117]. Moreover, it had been demonstrated also by previous studies that the ECM around cells in 3D models, can significantly impact cell proliferation, differentiation, mechano-responses, and cell survival [120].

Indeed both MTT and Alamar blue assay (**Figure 3a, 3b**), showed a time-dependent reduction of viability index only in 2D-HMTCs while, in 3D-HMTCs a slightly reduction was observed only after the early 24 hrs, instead in the following period of pulsed stress, an adaptation phenomenon with a homeostasis restoration was observed.

The apoptosis array revealed that 3D HTMCs were more able to counteract the pro-apoptotic proteins activation in response to daily H_2O_2 exposure, than the 2D model (**Figure 4a, 4b**). In fact, the significant increase of anti-apoptotic proteins such as Survivin, the pro-survival member of the Bcl-2 family, IGF1 and IGF2, was likely to sustain cell viability through apoptosis inhibition as already reported [121–125], despite the increase of caspase 3, BID and BAD. Moreover, the increase of TNFR1 levels suggested to us that also the pro-survival NF-kB transcription factor could be involved in this resistance to apoptosis [126].

In this regard, we also analysed the pro-inflammatory profile by cytokines gene expression and the NF-kB activation. Thus, after the first couple of H_2O_2 pulses the parallel activation of phosfo-NF-kB p65 and the expression of the inflammatory genes it controlled were not yet detectable, in both of models (**Figure 5 panel A,B,C,D, E**) probably due to a temporary NF-kB activation with no memory of the previous challenges and no signal accumulation visible by WB [127].

Conversely, in the 3D model after 72 hrs exposure the phospho-NF-kB subunits showed a marked and significant increase ($p<0.001$), compared to the control untreated cells and also to the 2D.

These effects suggested that in 2D model the HTMCs did not retain memory of the previous OS pulses even at 72 hrs while in the 3D model the NF-kB activation memory at last has been established leading to the onset of a chronic inflammatory response like *in vivo* condition [99]. Moreover, only in the 3D HTMC model a significant increase of IL1α ($p<0.05$) gene transcription was observed compared to the untreated 3D-HTMCs confirming the hypothesis of a mild temporany activation of the inflammatory pathway [127] after the first two pulses. However, at 72 hrs, all cytokines tested in the 3D model (IL1α, IL1β, IL-6) were significantly up-regulated with the corresponding NF-kB sustained activation at this time point.

These findings suggested that 3D-HTMC model, compared to 2D HTMC model, resembles physiologically TM features in vivo [99]. The TM-matrix embedded cells seem more sensitive to the OS reflecting in a more realistic way the OS role in TM degeneration which leads to the neuroinflammatory and glaucoma neurodegenerative outcomes.

1.2. Evaluation of different responses in 3D-HTMC in vitro models, under both static and dynamic culture conditions, after prolonged oxidative stress exposure

MATERIALS AND METHODS

1.2.1. Cell cultures

See paragraph 1.1.1

1.2.2. Dynamic 3D HTMC model

3D-HTMC were performed in LiveBox1, a transparent chamber provided by IVTech srl. Twenty-four hours after seeding, 3D-HTMC culture were submitted to a millifluidic circuit by connecting each perfusion chamber to a peristaltic pump able to maintain a constant growth medium flow rate of 70µL/min (LiveFlow, IVTech srl) for four days in order to allow the cell-to-cell interactions [128]. The flow rate has been set to overcome both diffusional limitations and soft gel degradation on 3D-HTMC (**Figure.6**).

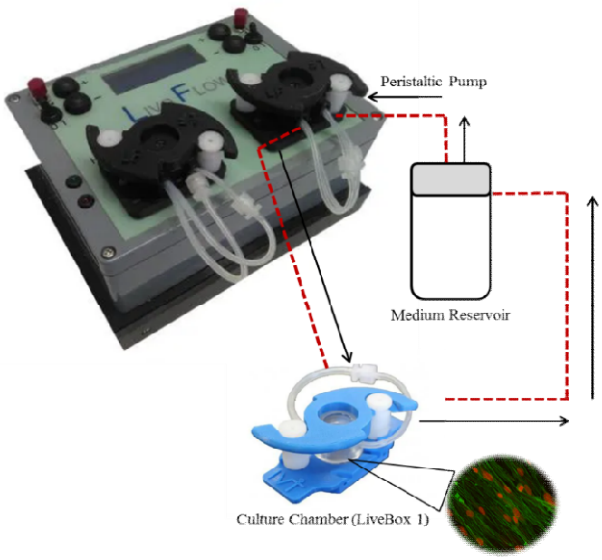

Fig.6: Perfusion bioreactor circuit diagram. The medium from medium reservoir is pumped by the action of the peristaltic pump, through the perfusion chamber where 3D-HTMCs were seeded, then it returns to the medium reservoir, completing the circuit. The image represents only one circuit, but the flow system includes two head pumps connected whit at least four perfusion chambers. (Kind permission of IvTech, Srl)

1.2.3. Experimental condition: prolonged oxidative stress exposure (168hrs) in 3D HTMC model under static and dynamic culture conditions.

Prolonged oxidative stress effect in both 3D-models lasted for a week (168 hrs) exposing once a day for 2 hours 3D-HTMCs to 500μM H2O2, followed by 22h of recovery, according to Poehlmann et al., 2013 and Kaczara et al., 2010 [110,129]. All molecular analyses on static and dynamic 3D-HTMC cultures were conducted once cells were freed from Corning® Matrigel® Matrix (Corning Life Sciences, Tewksbury, MA USA) by Corning Cell Recovery (Corning Life Sciences), according to the manufacturer's instructions.

1.2.4. Alamar Blue Assay

See paragraph 1.1.6

1.2.5. qPCR analysis

See paragraph 1.1.8

Primers used are shown in the **Table 3**.

GENE	GenBank	Forward	Reverse	Size (bp)
IL-1α	NM_000575.4	CAATCTGTGTCTCTGAGTATC	TCAACCGTCTCTTCTTCA	112
IL-1β	NM_000576.2	TGATGGCTTATTACAGTGGCAATG	GTAGTGGTGGTCGGAGATTCG	140
IL-6	NM_001318095.1	CAGATTTGAGAGTAGTGAGGAAC	CGCAGAATGAGATGAGTTGTC	195
MMP-1	NM_001145938.1	GGTGATGAAGCAGCCCAGATG	CAGAGGTGTGACATTACTCCAGG	187
MMP-3	NM_002422.5	TAATAATTCTTCACCTAAGTCTCT	AGATTCACGCTCAAGTTC	99
MMP-9	NM_004994.2	AACCAATCTCACCGACAGG	CGACTCTCCACGCATCTC	85
TNFα	NM_000594.4	GTGAGGAGGACGAACATC	GAGCCAGAAGAGGTTGAG	95
TGF-β2	NM_001135599.3	AACCTCTAACCATTCTCTACTACA	CGTCGTCATCATCATTATCATCA	149
Ubiquitin C	NM_021009.7	ATTTGGGTCGCAGTTCTTG	TGCCTTGACATTCTCGATGGT	50

Table 3. Primer sequences used for real time quantitative polymerase chain reaction analysis.

1.2.6. Human Apoptosis Array

See paragraph 1.1.7

1.2.7. Western Blot Analysis

See paragraph 1.1.9

1.2.8. Confocal Analysis

See paragraph 1.1.3.

1.2.9. Statistical Analysis.

Reported data are expressed as mean ± Standard Deviation (SD) and results were analyzed using two-way analysis of ANOVA for single comparison or two-way analysis of ANOVA variance followed by Bonferroni posttest for multiple comparisons. GraphPad Prism for Windows- version 5.03 and GraphPad Software, Inc., La Jolla, CA, USA) was used. Statistically significant differences were set at $p<0.001$; $p<0.01$; $p<0.05$.

Results

Alamar blue Assay

The effects of chronic 500μM H_2O_2 exposure were daily measured on 3D-HTMCs culture in static and dynamic conditions at each check point time up to 168 hrs, by Alamar Blue assay **(Figure. 7).**

After 24hrs of oxidative stress conditions, in 3D-static HTMC cultures the metabolic state showed a significant increase compared to untreated cultures (about 50%), and the reached levels in the following time exposure resulted in a time dependent decrease. After 24-48 hrs of prolonged oxidative stress, 3D-static HTMCs exhibited about 50 % increase of metabolic activity compared to the respective untreated cultures and 80% versus 3D-dynamic HTMCs. These effects decreased slowly during the following time exposures, and at 96 hrs the metabolic rate resulted similar to that of control cultures, and after 120 hrs of prolonged stress conditions, HTMCs exhibited a further impairment of metabolic state reaching lower values than those of untreated cultures. Instead, the metabolic trend of 3D-dynamic HTMCs did not evidence significant modulation within 24 hrs of applied stress. Nevertheless, over days, repeated OS exposure produced a significant drop of viability index (about 20% vs untreated dynamic cultures) that while remaining lower until 96 hrs, took to a slow recovery and starting from 144 hrs 3D-dynamic HTMCs showed a metabolic rate index similar to control cultures.

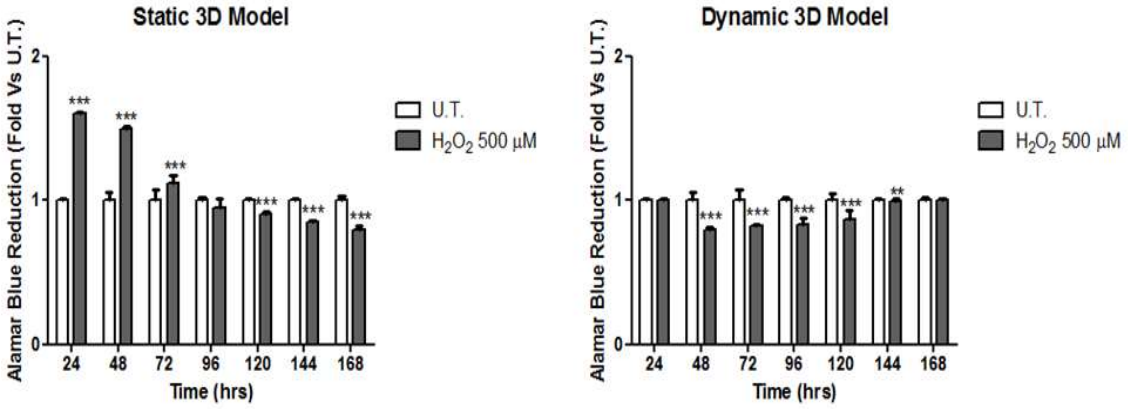

Fig. 7. HTMC metabolic state. Metabolic state of untreated (UT) and H_2O_2 treated 3D HTMCs cultured in static and dynamic conditions was analyzed by Alamar blue assay, during the last 4 hrs of the 22 hrs recovery time in between daily exposure to oxidative stressor. Data are expressed as "fold" Vs viability index of untreated 3D-HTMC, and each value represents the mean ± SD of 3 separate experiments running in triplicate. **p<0.01; ***p <0.001 vs untreated 3D-HTMCs (Two-way ANOVA).

q-PCR

In order to evaluate the pro inflammatory cytokines modulation and the MMPs regulation after OS treatment on 3D-HTMCs cultured in a static and dynamic manner, the cells were treated as mentioned above. The gene expression levels of IL-1α, IL-1β, IL6, TNFα, TGFβ, MMP1, MMP3 and MMP9 were analyzed by qPCR **(Figure. 8)**. At 48h only OS-treated 3D-dynamic HTMCs showed an up-regulation of IL1β, TGFβ, MMP1, MMP3 and MMP9, compared to untreated cultures, however 3D-static HTMCs did not evidenced a significant increase of markers investigated.

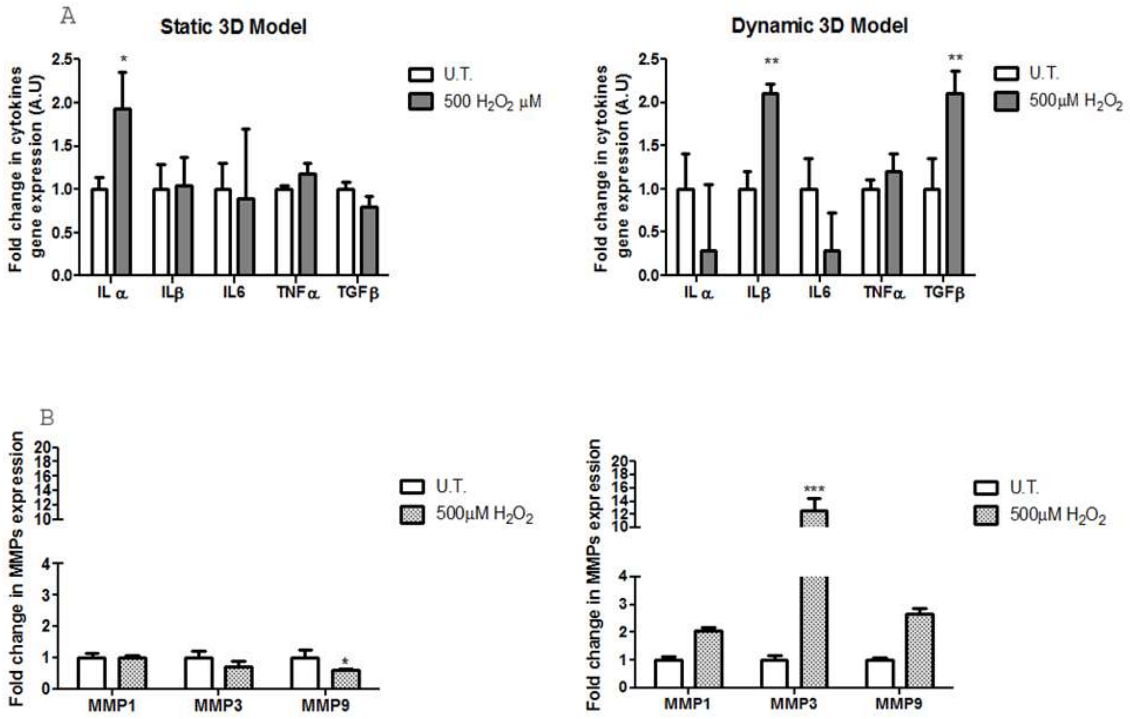

Fig. 8: qPCR. Quantitative PCR gene expression analysis of 3D-HTMCs cultured in static and dynamic conditions and subjected 500µM for 48h. IL-1α, IL-1β, IL6, TNFα and TGFβ (A), MMP1, MMP3 and MMP9 (B). Data are expressed as fold-increase relative to control at the same end-point and normalized to Ubiquitin housekeeping gene expression. Each bar represents the mean ± SD. of three independent experiments performed in triplicate. **p <0.01;*p<0.05; vs untreated 3D-HTMCs (Two-way ANOVA).

Human Apoptosis Array

After prolonged OS stress, multiple marker detection of apoptosis pathway was analyzed on both 3D-HTMC models by a microarray for 43 pro/anti apoptotic proteins. In **Figure. 8** we reported only the levels of those pro/anti-apoptotic proteins that resulted in significant modulation in almost one or in both 3D-HTMC models.

After 48 hrs OS exposure, 3D-static HTMCs evidenced a significant increase of pro-apoptotic BID, BIM, Caspase 3, p53, Smac, TNF-R1 proteins (**Figure. 8, A**). This modulation resulted more marked after 72 hrs for above proteins, except for proapoptotic p53 and Smac. Regarding antiapoptotic molecules, the OS exposure after 48hrs resulted in a significant increase Survivin, IGFBP1 and IGF1, and after 72 hrs, a stronger increase of BCL2, BCLw, survivin, x IAP, CD 40 and IGF1. These modulations of pro and anti-apoptotic markers are lapsed in 3D-static cultures at 168 hrs,

In dynamic conditions, after 48 hrs of OS stimulus, pro-apoptotic BAD, BID, BAX, BIM, CytoC, Smac and TNFα, TNFα/TNFR1, TNFα/TNFR2 protein levels were significantly increased compared those of control cultures. At 72 hrs the levels of almost all markers were at basal levels, except for TNFα, TNFα/TNFR1, TNFα/TNFR2 which rose in a time dependent way until 168 hrs. As for anti-apoptotic patterns, only IGFBP1 evidenced a significant increase after 48 hrs, while BCL2, BCLw, Hsp70, CD40, IGFBP1 and IGF1 showed up to 3 fold increase after 168 hrs.

A

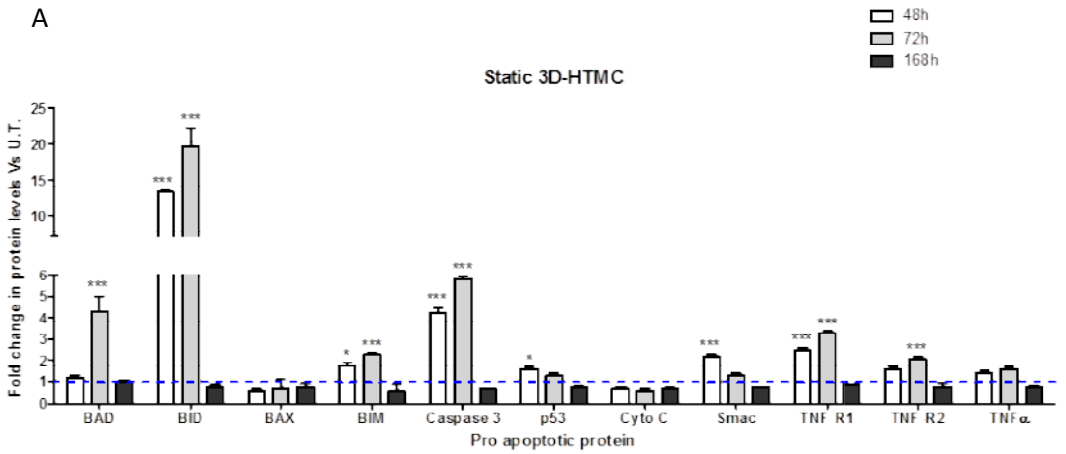
48h
72h
168h
Static 3D-HTMC
Fold change in protein levels Vs U.T.
BAD
BID
BAX
BIM
Caspase 3
p53
Cyto C
Smac
TNF R1
TNF R2
TNF α
Pro apoptotic protein

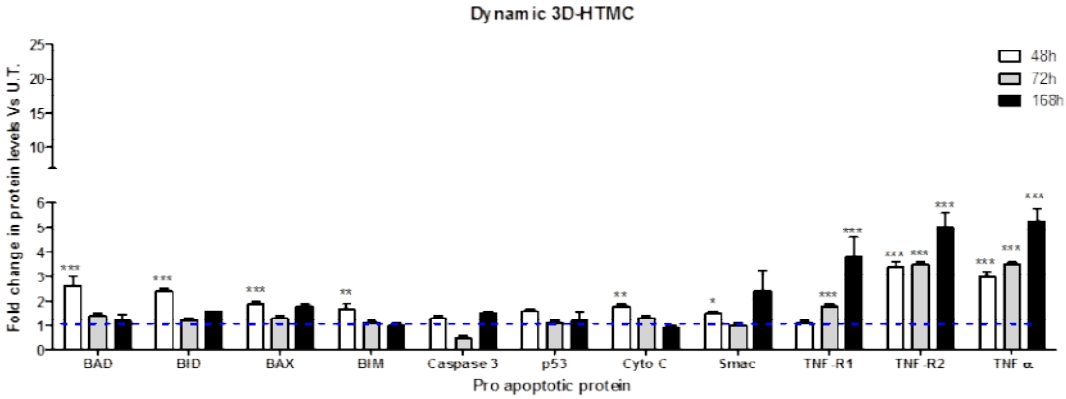
Dynamic 3D-HTMC
48h
72h
168h
Fold change in protein levels Vs U.T.
BAD
BID
BAX
BIM
Caspase 3
p53
Cyto C
Smac
TNF R1
TNF R2
TNF α
Pro apoptotic protein

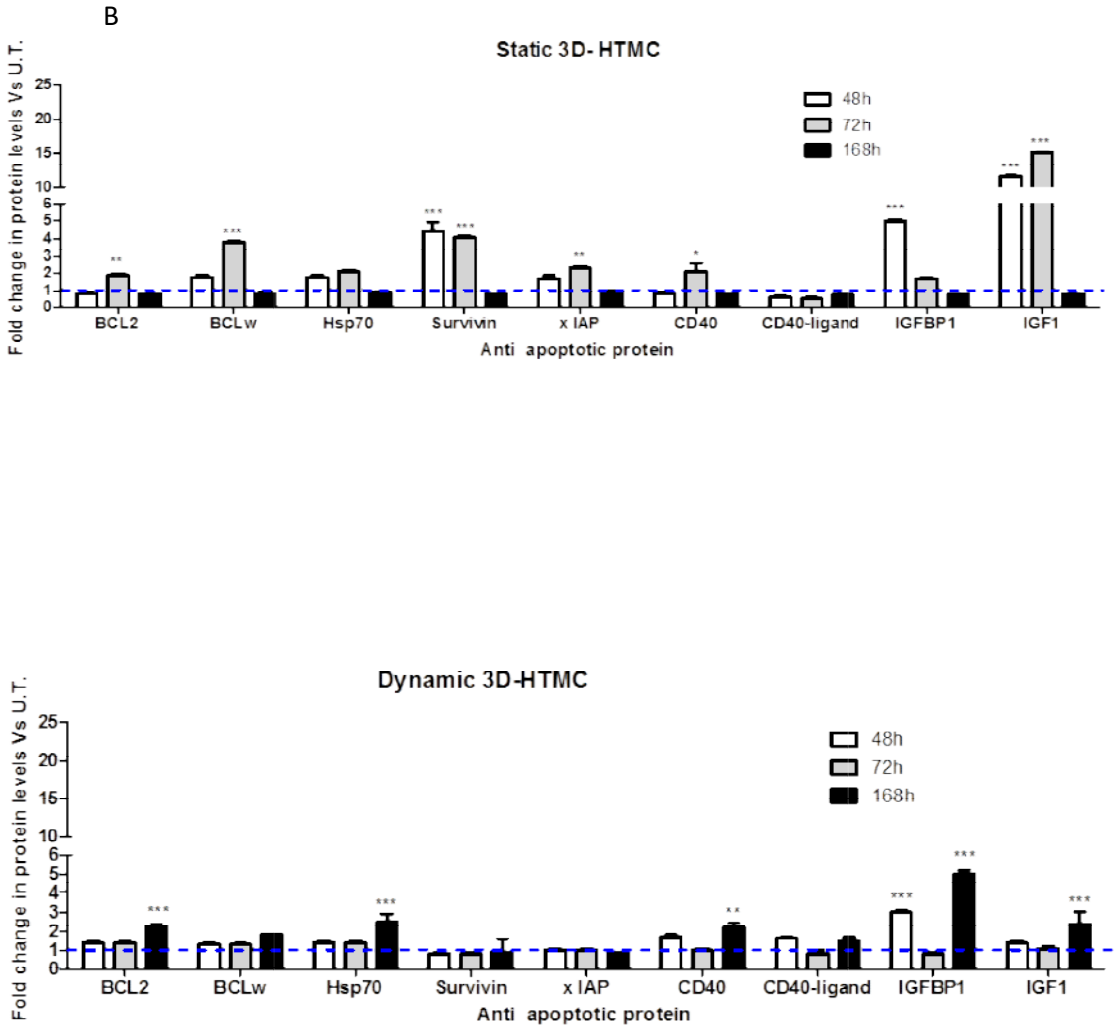

Fig. 8: Apoptosis array. Analysis of pro- and anti- apoptotic protein levels (Panel A and Panel B, respectively) in 3D-HTMCs cultured in static and dynamic conditions, were performed after 48-72-168hrs of 500μM H_2O_2, by Human Antibody Array C1 (RayBio® C-series). In the graphs only the analysis of the markers significantly modulated were reported. The light blue dotted line represents the protein level of untreated HTMC for each protein examined. Twelve individual models were arrayed (six static 3D-HTMCs plus six dynamic 3D-HTMC) and per experiment the intensity of Positive Control Spot was used to normalize signal responses for comparison of results across multiple arrays. *$p<0.05$; ** $p<0.01$; ***$p<0.001$ vs. respective untreated cultures (One-way ANOVA).

Western Blot Analysis

The analysis of PARP-1 full length-cleavage was performed on 3D-HTMCs, after 168 hours of exposure to chronic pro-oxidant stimulus (500μM H_2O_2) **(Figure. 9, A).** Chronic exposure to H_2O_2 exerted opposite effects on 3D-HTMCs depending on the culture conditions, in fact, a marked and significant increase of PARP-1 cleavage levels was detected only in 3D-HTMCs static cultures, while in dynamic models 3D-HTMCs PARP-1 expression got a full length. NF-kB transactivation, as an inflammatory / antiapoptotic response marker, was analyzed in terms of the ratio between the levels of phospho-NF-kB p65, the activated form of NF-kB, versus total NF-kB **(Figure 9, B)**. A remarkable NF-kB activation occurred only in 3D-HTMC cultured in dynamic conditions.

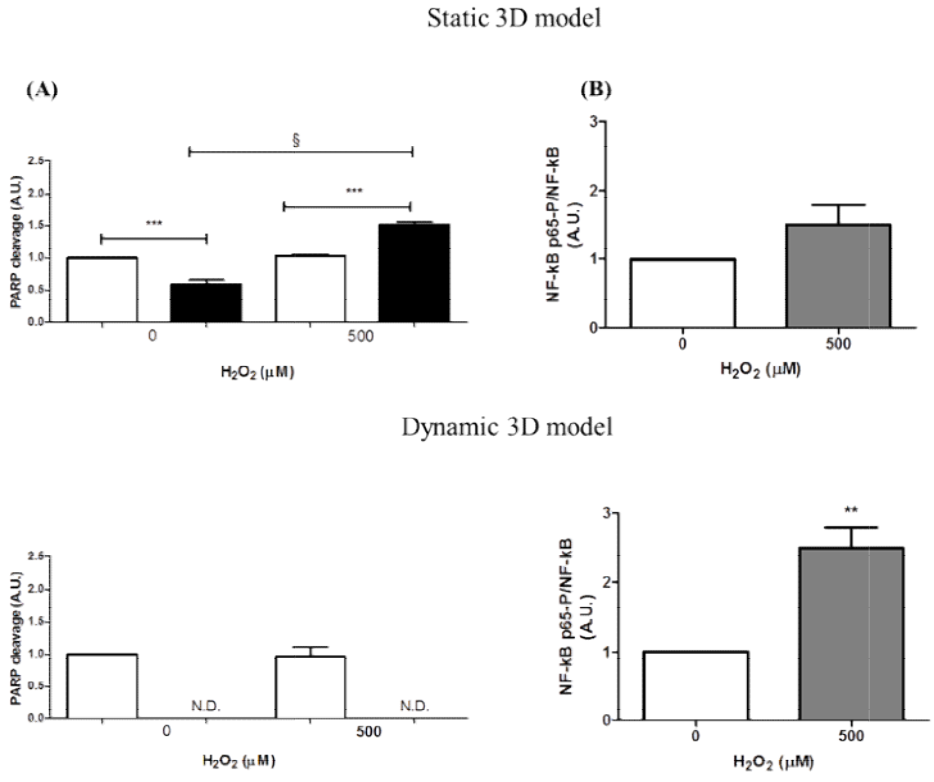

Fig. 9: PARP1 cleaved levels and NF-kB levels in 3D- HTMC static and dynamic cultures after 168hrs of chronic oxidative treatment. The analysis was performed by immunoblotting and the bars represent the both ratio of cleaved PARP1 and phosfoNF-kBp65/NF-kB, and are expressed as arbitrary units (AU). Data represent the mean ± SD of 2 independent experiments, running in triplicate. *** p <0.0001; **p<0.01 vs. untreated 3D cultures and §p<0.0001 3D-HTMC treated vs 3D-HTMC control cultures (Two-way ANOVA).

Confocal analysis

After 168 hrs of experimental procedures, spatial organization of 3D-HTMCs cultures was analyzed by confocal microscopy (**Figure. 10**).

In the 3D- static HTMC cell imaging reconstruction it can be observed that the actin microfilaments, detected by fluorescent probe FITC-Phallodin, resulted uniformly distributed in parallel lines along with the longitudinal axis and a lot of cell-to-cell interaction was detected. However, in dynamic 3D-HTMCs imaging reconstruction, actin microfilaments showed less orderly distribution of the cells embedded in the matrix. In both culture conditions, the H_2O_2- treated 3D-HTMCs showed an increase of nuclear size, labeled by fluorescent probe To-Pro^{TM}, while actin microfilament became thickened, tense and distributed in radial manner only in dynamic conditions.

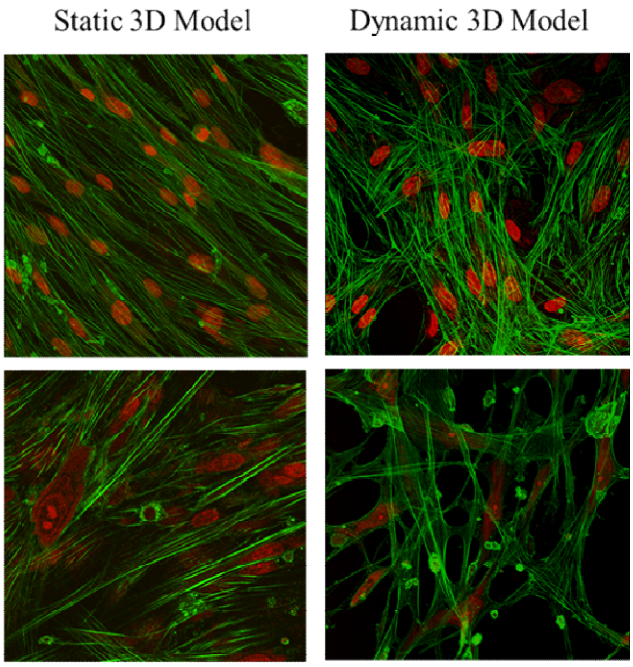

Fig. 10: Confocal analysis. Confocal microscopy analyses of nucleus and cytoskeletal markers were performed on untreated and H_2O_2-treated 3D-HTMCs in static (on the left) and in dynamic (on the right) conditions after 168 hours of experimental procedures. Representative images are related to immunoreactivity for To-Pro^{TM} and Phalloidin, as nuclear and cytoskeleton markers, respectively. Merged images showed cytoskeleton plus Nucleus. Fluorescence signals were captured at 60x magnification.

Conclusions

As reported in the above study, we have been demonstrated the reliability of the 3D culture model to assess a realistic HTMC model. However, to further increase the 3D-HTMC complexity, we approached to the millifluidic technique. Indeed, in the last few years 3D-cultures together with 3D-culture techniques have represented important steps towards in vitro models ever more physiologically relevant and useful for disease species-specific studies. In particular, the addition of a perfusion flow ranging from milli- to micro-fluidic techniques have implemented the performance of standard 3D-cultures. Duval et al. (2017) reported that cells and tissues cultured in vitro, under specific conditions, maintain power law metabolic scaling in cultures proving the physiological relevance for these downscaled in vitro systems [116].

Taking in account these results, we analyzed the 3D-static and dynamic HTMC culture morphology by confocal microscopy at the end of chronic OS exposure (**Figure.10**). The F-actin was chosen as cytoskeleton indicator because resulted abundant in TM cells. In our experimental conditions, after 168 hrs exposure to oxidative stressor, in dynamic 3D-HTMCs cultures actin microfilaments appeared thinned and nuclear size resulted in an enlargement compared to that of untreated cultures.

Considering these observations together, it can be argued that chronic OS induced an F-actin cytoskeleton reorganization and altered the cell adhesive properties of 3D-HTMCs. As occurs during glaucoma, the TM cells undergo diffuse injury, with increased oxidative stress leading to both an alteration of motility of the entire TM and an alteration of the barrier; this scenario subsequently leads to an increase in IOP [130].

The molecular damage related to OS in both 3D-HTMC models was investigated through the amplification of five cytokines including IL1α, IL1β, IL6, TNFα and TGFβ, by qPCR.

After 48hrs of experimental stress conditions, we found a significant up-regulation of TGF-β1 and IL-1β, two crucial markers involved in ECM remodeling by regulating the autophagic signal pathway [131,132] and acute inflammatory response in several diseases including glaucoma eyes [133], only in dynamic 3D-HTMC cultures. Therefore, the increase of these two cytokines by the OS is relevant because the impairment of the trabecular reticulum motility is one of the first molecular events of glaucoma occurrence (**Figure. 8A**).

Moreover, we also evaluated the MMPs gene amplification because, as known, their enhanced activation could play a central role both in the remodeling of ECM during the ocular growth and development and in remodeling TM ECM to counteract the outflow resistance and IOP in glaucoma [134,135]. In this regard, I investigated the gene expression of MMP1 and MMP3 in both culture models but only in 3D-dynamic cultures they were up regulated by the pro oxidant stimulus, underlining how more physiological culture conditions are able to better mimic the homeostatic TM cell responses found in vivo to adjust the outflow resistance [136,137].

Furthermore, 3D-HTMC models, compared to the standard 2D cultures commonly used for *in vitro* glaucoma studies, showed to maintain the tissue architecture polarity which represents an important hallmark for the tissue function maintenance found in vivo. However, a dynamic environment allows a better maintenance of cell structures than static culture conditions, also confirmed by confocal analysis, and this capability better supported the cellular polarization, sustaining, as a consequence, a long-term viability of the cells. Indeed, the modulation of apoptosis markers and NF-kB protein levels in 3D-dynamic HTMC cultures showed a more efficient adaptive response over time to OS-damage, compared to 3D-static models [138], triggered the inflammation cascade, as it happens in vivo during glaucoma occurrence.

Then, in 3D-dynamic HTMCs we observed an increase of pro apoptotic proteins including BAD, BIM, BID, and cytochrome C only in early time of pro-oxidant stimulus exposure and a gradually increase over time of TNFα and its receptor 1 (TNFR1). However, a stronger increase at 168hrs of anti-apoptotic markers, as survivin and IGFPB1 and in a way also TNFR2 (TNF receptor 2), that acts as cell proliferation activator, was found to counterbalance the apoptotic response (**Figure. 8B**). Moreover, these results together with the uncleaved PARP1, the increase of phosfoNF-kBp65 rate compared to total NF-kB level and the healthy metabolic state were in favour of cell survival rather than apoptosis.

On the other hand, 3D- static HTMC cultures evidenced an overexpression of BAD, BID and Caspase 3 and to a lesser extent also of TNRF1 and also a marked induction of anti-apoptotic proteins such as BCL2, BCLw, survivin, x IAP, CD 40 and IGF1 up to 72hrs of OS-exposure. Nevertheless after 168hrs to prolonged sub-toxic stress exposure we reported PARP1 cleaved, no activation of NF-kB and a reduced metabolic cell state leading to hypothesize that 3D-static HTMCs carried on to apoptosis pathway (**Figure 9**) [139,140].

As reported by Duval et al. (2017), cells and tissues cultured *in vitro*, under specific conditions, maintain power law metabolic scaling in cultures proving the physiological relevance for these downscaled *in vitro* systems [141]. Moreover, the cross-talk between cells allows to condition their habitat so as to interact with each other (i.e. cytokines secretion) by promoting cell survival and proliferation, in a more realistic manner even after stimuli, such as oxidative stress. In conclusion, in our study the 3D-in vitro model exploiting a millifluidic technology turns out to be a useful tool providing a physiological cellular environment under controlled experimental conditions.

2nd task: Effects of flow pressure increase on 3D HTMC dynamic model, whereas the increase in IOP is one of the main risk factors of glaucoma.

MATERIALS AND METHODS

2.1. Cell Cultures

See paragraph 1.2.1

2.2. Experimental conditions: applying of flow pressure increase in dynamic 3D - HTMC models.

In order to mimic the IOP-increase Live Pa (IVTech srl), an auxillary device, was connected to bioreactor system up to 168hrs (**Figure.11**) . Live Pa increases by 10% the culture chamber pressure thanks to a plunger which compress the output pipe of LiveBox1. Indeed, following the allometric calculation scale [128,141], the value of pathological pressure derived from the basal pressure of the bioreactor was 100µl/min=0.02KPa. So, the pathological pressure was 100µl/min= 0,022 kPa.

By this way, 3D-HTMCs were mainatained for 24 hrs/day under dynamic conditions and for 12hrs/day were submitted to an increase of flow pressure, following the circadian rhythm. All molecular analyses on dynamic 3D-HTMC cultures were conducted once cells were freed from Corning® Matrigel® Matrix (Corning Life Sciences, Tewksbury, MA USA) by Corning Cell Recovery (Corning Life Sciences), according to the manufacturer's instructions

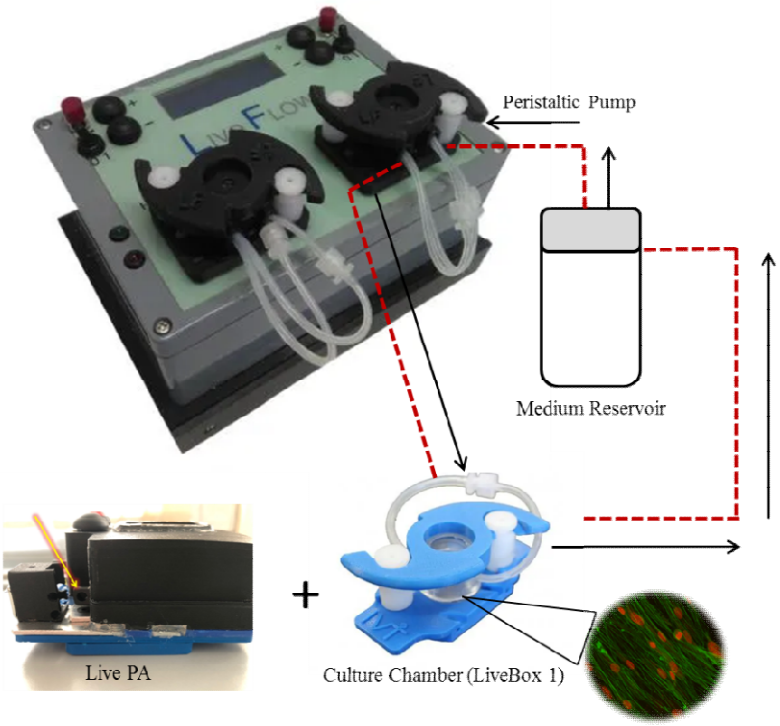

Fig.11: **Perfusion bioreactor circuit diagram plus Live Pa.** The medium from medium reservoir is pumped by the action of the peristaltic pump, through the perfusion chamber where 3D-HTMCs were seeded. The plunger of Live PA, indicated by the arrow, press the output pipe of Live Box1, increasing the pressure inside the chamber. (Kind permission of IvTech srl)

2.3. Alamar Blue Assay

See paragraph 1.2.4

2.4 Confocal Analysis

See paragraph 1.2.8

2.5 qPCR analysis

See paragraph 1.2.5. Primers used are shown in the **Table 4**.

GENE	GenBank	Forward	Reverse	Size (bp)
Alpha-SMA	NM_001141945.1	TTGAGAAGAGTTACGAGTTG	GGACATTGTTAGCATAGAGG	189
Collagen 1A	NM_000088.3	CTTTGCATTCATCTCTCAAACTTAGTTTT	CCCCGCATGGGTCTTCA	163
Myocilin	NM_000261.2	GTTACCACAAGCCACAAT	GAAGCATTAGAAGCCAACT	112
MMP-1	NM_001145938.1	GGTGATGAAGCAGCCCAGATG	CAGAGGTGTGACATTACTCCAGG	187
MMP-3	NM_002422.5	TAATAATTCTTCACCTAAGTCTCT	AGATTCACGCTCAAGTTC	99
MMP-9	NM_004994.2	AACCAATCTCACCGACAGG	CGACTCTCCACGCATCTC	85
SPARC	NM_003118.4	ATGGTTCCTGTAAGCACTAA	TGAATGAATGAATGAATGAATGC	143
TGF-beta2	NM_001135599.3	AACCTCTAACCATTCTCTACTACA	CGTCGTCATCATCATTATCATCA	149
IL-1alpha	NM_000575.4	CAATCTGTGTCTCTGAGTATC	TCAACCGTCTCTTCTTCA	112
IL-1beta	NM_000576.2	TGATGGCTTATTACAGTGGCAATG	GTAGTGGTGGTCGGAGATTCG	140
IL-6	NM_001318095.1	CAGATTTGAGAGTAGTGAGGAAC	CGCAGAATGAGATGAGTTGTC	195
Ubiquitin C	NM_021009.7	ATTTGGGTCGCAGTTCTTG	TGCCTTGACATTCTCGATGGT	50

Table 4. Primer sequences used for real time quantitative polymerase chain reaction analysis.

2.6 Western Blot Analysis

See paragraph 1.2.7

2.7 Statistical Analysis

Reported data are expressed as mean ± Standard Deviation (SD) and results were analyzed using two-way analysis of ANOVA for single comparison or two-way analysis of ANOVA variance followed by Bonferroni posttest for multiple comparisons. GraphPad Prism for Windows- version 5.03 and GraphPad Software, Inc., La Jolla, CA, USA) was used. Statistically significant differences were set at $p<0.001$; $p<0.01$; $p<0.05$.

Results

Alamar blue Assay

The effects of pathological pressure on 3D-HTMCs, were daily measured up to 168 hrs, by Alamar Blue assay **(Figure. 12).** Therefore, the metabolic activity of 3D-HTMCs subjected to the pressure increase, shown a slightly decrease compared to the untreated 3D-HTMCs for all experimental time.

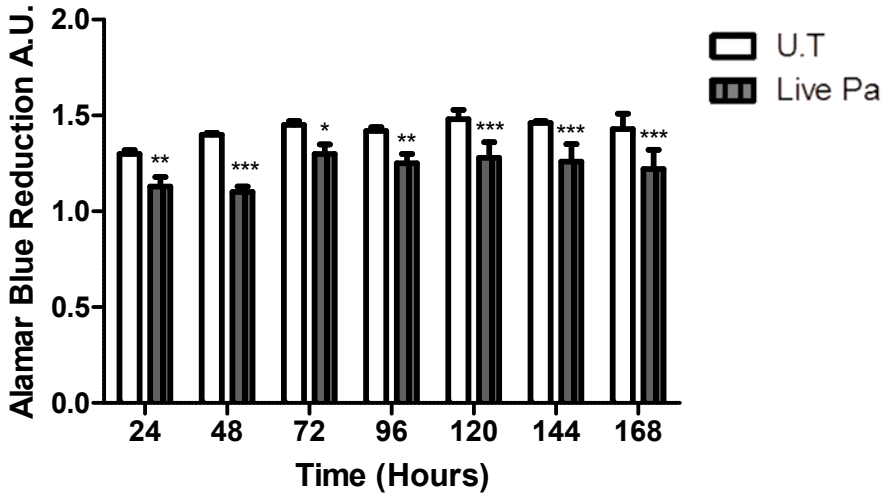

Fig. 12. HTMC metabolic state. Metabolic state of untreated (UT) and pathological pressure treated 3D HTMCs cultured in dynamic conditions was analyzed by Alamar blue assay, after pathological pressure treatment. Data are expressed as "fold" Vs viability index of untreated 3D-HTMC, and each value represents the mean ± SD of 3 separate experiments running in triplicate. ***p <0.001 ;**p<0.01*;p<0.05; vs untreated 3D-HTMCs (Two-way ANOVA).

Confocal analysis

In order to evaluate the morphological changes which occurred in the 3D-HTMC after increase of pressure, confocal analysis was performed at168 hrs.

As known the F-actin bundles which constitute the microfilaments, under physiologic conditions regulate cell shape, phagocytosis, contraction, and motility. However, in glaucomatous TM the F-actin bundles are less linear and organized by giving a cytoskeleton disorganization.

In Figure 13, in response to pathological pressure exposure, 3D-HTMC cell imaging reconstruction evidenced a different distribution of actin structure, nuclear size and an increased ECM, compared to 3D-HTMC cultures control.

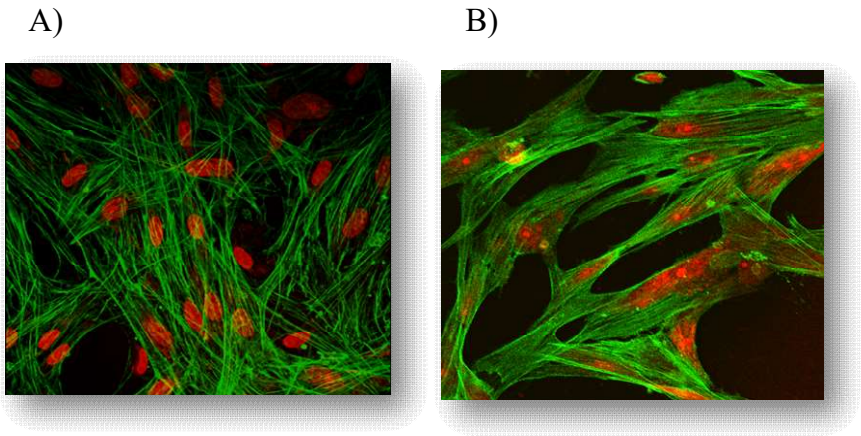

Fig.13: Morphological changes in 3D-HTMC cytoskeleton. Confocal microscopy analyses of nucleus and cytoskeletal markers were performed on 3D-HTMC cultures control and 3D-HTMC (A, and B, respectively) subjected to pathological pressure after 168 hours of experimental procedures. Representative images are related to immnuoreactivity for To-ProTM and Phalloidin, as nuclear and cytoskeleton markers, respectively. Merged images shown cytoskeleton plus Nucleus. Fluorescence signals were captured at 60x magnification.

qPCR analysis

qPCR analysis for pro inflammatory, pro fibrotic and ECM remodeling markers was performed on 3D-HTMC at 72hrs of experimental conditions of increase of flow pressure, as mentioned above .

The high pressure stimulated the mRNA expression of SPARC, COL1A1, α-SMA, MYOC, TGFβ and also of TNFα, ILβ, MMP1 and MMP3. Indeed, this mechanical stimulus acts as important biological processes in ECM turnover and pro-inflammatory cytokines, and it be associated with TM fibrosis and cell function impairement (**Figure. 14 A,B,C,D**)

Western Blot Analysis

NF-kB transactivation, as an inflammatory / antiapoptotic response marker, was analyzed in terms of the ratio between the levels of phospho-NF-kB p65, the activated form of NF-kB, versus total NF-kB **(Figure 14, E)**. A slightly increased of NF-kB activation occurred in 3D-HTMC undergone to pathological pressure.

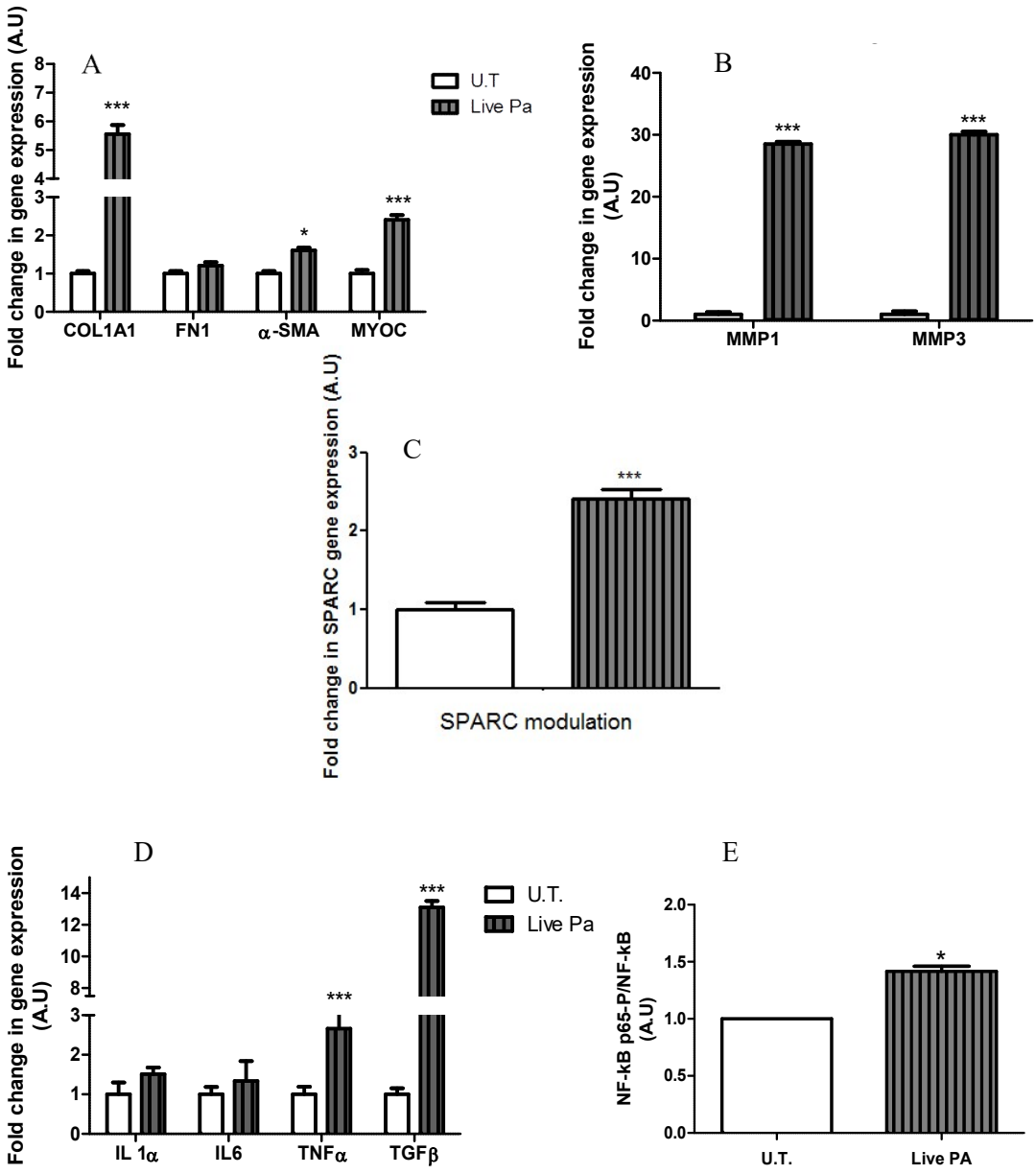

Fig.14: ECM and pro-inflammatory cytokines gene regulations and NF-kB activation. Quantitative PCR gene expression analysis of 3D-HTMCs cultured dynamic conditions and subjected to. COL1A1, FN1, α-SMA, MYOC (A), MMP1, MMP3 and TIMP-1 (B), SPARC (C) IL-1α, IL-1β, TNFα and TGFβ (D). Data are expressed as fold-increase relative to control at the same end-point and normalized to Ubiquitin housekeeping gene expression. Each bar represents the mean ± SD. of three independent experiments performed in triplicate. **NF-kBp65** activation was evaluated in HTMC cells subjected to pathological pressure for 168 hrs. The analysis was performed by immunoblotting and the bars represent the ratio of phosfoNF-kBp65/NF-kBp65, and are expressed as fold vs. untreated HTMC cultures. Data represent the mean ± S.D. of 3 independent experiments.

***p<0.001;**p <0.01;*p<0.05; vs untreated 3D-HTMCs (Two-way ANOVA).

Conclusions

Our 3D-HTMC dynamic model with the Live Pa as auxillary device, was able to reproduce the main of pressure increase effects on TM cellular dysfunction which is the primary site of resistance to aqueous humor outflow [142]. Indeed, stimuli including mechanical stretch and/or OS damage, induce the the activation of TM signaling pathways which lead to several changes in ECM turnover, gene expression or the abnormal NF-κB family members expression [142–145]. Indeed it was reported that an excessive ECM deposition in TM, contributes to lost the IOP homeostasis. Therefore, the identification of factors involved in the dynamic balance of synthesis and degradation of ECM is of great importance, also at a pharmacological level [4,146].

As shown in **Figure. 13**, the mechanical stretch induced by increased pressure has determined in 3D-HTMC both the thickening of F-actin fibers and the cytoskeleton reorganization, compared to the F-actin structures and the organized cytoskeleton of 3D-HTMC under normal dynamic conditions.

Moreover, the molecular changes evoked by the increase of pressure in 3D-HTMC were analysed by several gene expression including MMPs which are necessary to maintain outflow facility and pro inflammatory and pro fibrotic markers. So, the ECM turnover in our model was sustained by the marked increase of MMP1 and MMP3 and by synergism between TNF-α and IL-1β up-regulation (**Figure 14, D**) [147]. However, the increase of SPARC amplification [146], that is a key factor in the ECM remodeling [148], promoted the activation of TGF-β signaling pathway and the COL1A1 up-regulation which have been identified as a possible pathogenic factor responsible for POAG [153,154].

In addition, it was given evidence that the activation of inflammatory stress response via IL-1/NF-kappaB ~~found~~ in several forms of glaucoma, seems to be regulated by a negative

feedback loop thought the endogenous MYOC over-expression [149]. Therefore, in our model the increase of pressure induced the MYOC up regulation without showing the effects of complete negative feedback loop because the NF-kB protein levels were significantly increased after 168hrs, compared to 3D-HTMC maintained under standard dynamic conditions (**Figure. 14 A**).

Thus, we assumed that this pathological model described all the main features of TM dysfunction found in glaucomatous patients, after the increase of IOP.

3rd task: Evaluation of the usefulness of the proposed in vitro platform to check the effectiveness of targeted therapies

In order to assess the suitability of our milliluidic platform for screening efficacy of therapeutic approaches, we analysed the effects of a concentrated polyphenol mixture in counteracting the effects of OS and of flow pressure increase on dynamic 3D-HTMCs. The relevance of our 3D HTMC, in dynamic condition, with bioreactor system model as in vitro platform for assessing the efficacy of chemical drugs, we analysed the effects of a concentrated polyphenol mixture, after OS and increase of flow pressure. iTRAB® (**Figure.1**5) is a patented formulation derived from Perilla extracts and it is a concentrated mixture of polyphenols ≥ 2.5%, with a high lipophilia and among its components there are catechins and fatty acids that are known to counteract the OS damage. In a previous study [74] iTRAB® was tested on 2D-HTMC model and it has been proven the antioxidant effects of compound with a directly controls the oxidative damage to TM and its high trans-corneal bio- availability.

iTRAB® was tested on dynamic 3D-HTMC model under prolonged OS and under pathological pressure, two of the main POAG risk factors.

MATERIALS AND METHODS

3.1. Cell Cultures

See paragraph 1.2.1

Fig.15. DRAIN drops® is an ophthalmic solution based on iTRAB® (high concentration polyphenols in hyaluronic acid)

3.2. Experimental conditions

The experimental working iTRAB ® solution was obtained by dissolving dry perilla extract in TMGM (0.15% final concentration, v/v), conforming to the informations of iTRAB® protocol

Prolonged OS+ iTRAB®: 3D-HTMCs were daily treated for 2 hrs, in a static manner, with 500µM H_2O_2 (as already mentioned in the first part), then, after removal of the experimental medium, HTMC were exposed to iTRAB ® at the 0.15% in TMGM for 2 hrs. Later the HTMCs were cultured with the fresh media for further 20 hrs in dynamic conditions.

Increased Flow Pressure + iTRAB®:3D-HTMC were submitted to IOP increase following the circadian rhythm for up to 72 hrs. After a daily complete pressure cycle, iTRAB ® working solution was added into culture, in a static manner, for 2 hrs. Subsequently, the cells were cultured with the fresh media for 22 hrs in dynamic conditions.

3.3. DCF Assay

See paragraph 1.1.5

3.4. Alamar Blue Assay

See paragraph 1.2.4

3.5. qPCR Analysis

See paragraph.1.2.5 . Primers used are shown in the **Table 1.**

GENE	GenBank	Forward	Reverse	Size (bp)
IL-1α	NM_000575.4	CAATCTGTGTCTCTGAGTATC	TCAACCGTCTCTTCTTCA	112
MMP-1	NM_001145938.1	GGTGATGAAGCAGCCCAGATG	CAGAGGTGTGACATTACTCCAGG	187
MMP-3	NM_002422.5	TAATAATTCTTCACCTAAGTCTCT	AGATTCACGCTCAAGTTC	99
MMP-9	NM_004994.2	AACCAATCTCACCGACAGG	CGACTCTCCACGCATCTC	85
TNFα	NM_000594.4	GTGAGGAGGACGAACATC	GAGCCAGAAGAGGTTGAG	95
TGF-β2	NM_001135599.3	AACCTCTAACCATTCTCTACTACA	CGTCGTCATCATCATTATCATCA	149
Alpha-SMA	NM_001141945.1	TTGAGAAGAGTTACGAGTTG	GGACATTGTTAGCATAGAGG	189
Collagen 1A	NM_000088.3	CTTTGCATTCATCTCTCAAACTTAGTTTT	CCCCGCATGGGTCTTCA	163
Myocilin	NM_000261.2	GTTACCACAAGCCACAAT	GAAGCATTAGAAGCCAACT	112
Fibronectin (FN1)	NM_002026	CCAgCAgAggCATAAggTTC	ggTCAAAgCACgAgTCATCC	95
Ubiquitin C	NM_021009.7	ATTTGGGTCGCAGTTCTTG	TGCCTTGACATTCTCGATGGT	50

Table 1. Primer sequences used for real time quantitative polymerase chain reaction analysis.

3.6. Human Apoptosis Array

See paragraph 1.1.8

3.7. MTT Assay

See paragraph 1.1.5

Results: Effects of ITRAB on OS

DCF assay

The fluorometric DCF assay was performed in order to evaluate the ability of hydrogen peroxide to induce ROS production in dynamic 3D-HTMC cultures and how the iTRAB® counteracts this production. The ROS production was quantified after 2 hrs with and without the addition of iTRAB® (**Figure 16**). A different ROS production after the addition of iTRAB® that's clear: dynamic 3D-HTMC cultures decreased their intracellular ROS production by about 300 %

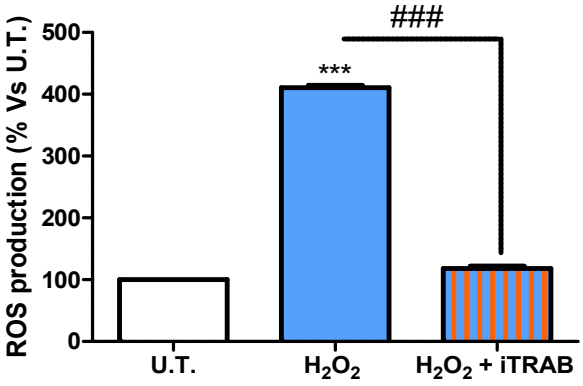

Fig.16: DCF Assay. DCF assay were performed after 2 hrs of experimental procedures. Data are expressed as % of U.T. 3D-HTMC and represent the mean ± SD of 3 indipendent experiments. ***p<0.001 vs UT; ### p< 0.001 vs H2O2 + iTRAB®. (Two-way ANOVA followed by Bonferroni's test).

Alamar Blue Assay

The effects of prolonged 500µM H2O2, iTRAB® and 500µM H_2O_2 + iTRAB® exposure on dynamic 3D-HTMC were measured at each check point time up to 72 hrs, by Alamar Blue assay (**Figure. 17**). 3D HTMC exposed to chronic stress reflected a decrease of resorufin reduction until 72 hrs. Conversely, untreated 3D HTMC cultures showed a constant increase of metabolic activities and even during iTRAB® treatment. Overall, at all time points, the treated by 500µM H2O2 + iTRAB® 3D HTMCs evidenced an increase of their metabolic state as opposed to H2O2 exposure. This increment increased slightly after 72 hrs of treatment, whilst remaining lower than untreated cells.

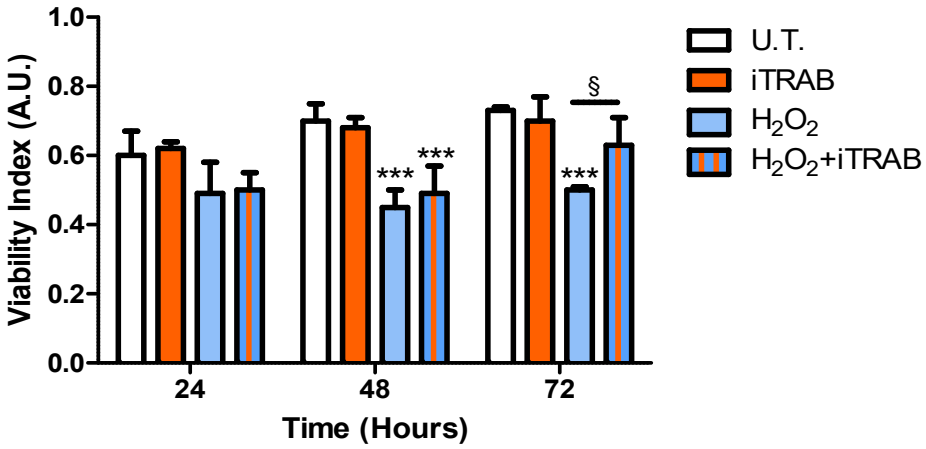

Fig.17: HTMC metabolic state.Viability indices were performed by Alamar blue assay.Data are expressed as Arbitrary units (AU). Each value represent the mean ± S.D of 2 separated experiments running in triplicate. ***p<0.001 Vs U.T.; § p<0.05 Vs H_2O_2 plus iTRAB® (Two-way ANOVA followed by Bonferroni's test)

qPCR analysis

In order to evaluate the iTRAB® effects in countering the inflammatory stimulus of H_2O_2 on dynamic 3D-HTMCs, the cells were treated for **72 h** prior to performing inflammatory gene expression profiling. The gene expression levels of IL-1α, TNF-α, TGF-β and MMP-1,3 and 9 were analysed by qPCR (**Figure. 18A**). At 72 hrs, the 3D-HTMCs treated with a pro-oxidant stimulus showed an increased of all cytokines compared to HTMCs untreated. Moreover, at this time point, 3D-HTMCs treated with iTRAB® revealed a slight, but significant decrease of pro-inflammatory cytokines. Also the TGF-β gene expression, a pro-fibrotic cytokines, decreased after treatment with iTRAB® compared to the 3D-HTMCs treated with H_2O_2 **(Figure.18B).**

Conversely, the MMP-1 MMP-3 gene expression showed a marked increase about 2 and 3 fold respectively, after iTRAB® treatment compared to H_2O_2 3D-HTMC treatment **(Figure.18C)**.

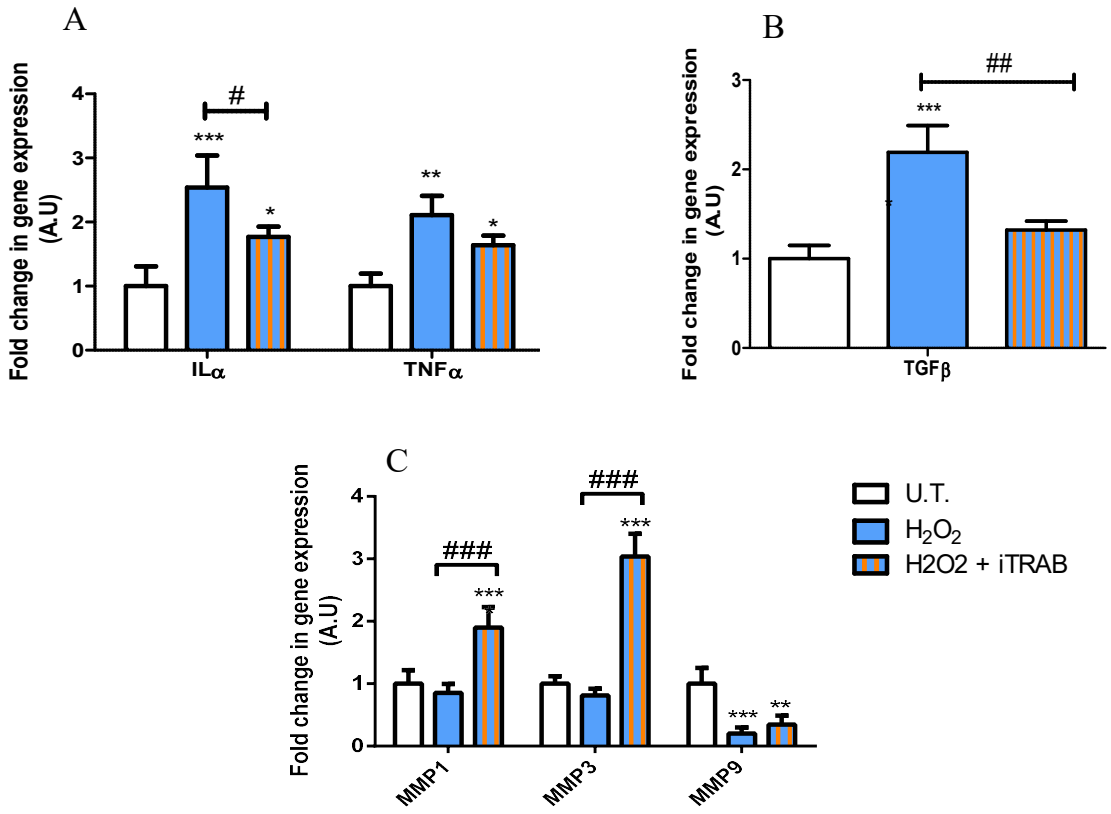

Fig.18. Gene expression. Quantitative PCR of IL1-α, TNF- α, TGF-β, MMP-1, MMP-3 and MMP-9 was performed at 72 hrs. Data are expressed as fold-increase relative to U.T. at the same end-point and normalized to Ubiquitin housekeeping gene expression. Each bar represents the mean ± s.d. of three independent experiments performed in triplicate. ***p<0.001; **p<0.01; *p<0.05 vs U.T. ### p<0.001; ##p<0.01; #p<0.05 vs. H2O2 + iTRAB®(Two-way ANOVA followed by Bonferroni's test)

Apoptosis Array

After prolonged OS stress followed by iTRAB® treatment, multiple marker detection of apoptosis pathway was analyzed on dynamic 3D-HTMC models by a microarray for several pro-apoptotic proteins. In **Figure.19** we reported only the levels of those anti-apoptotic proteins that resulted in significant modulation. iTRAB® would seem capable to counteracting the apoptosis in dynamic 3D-HTMC model.

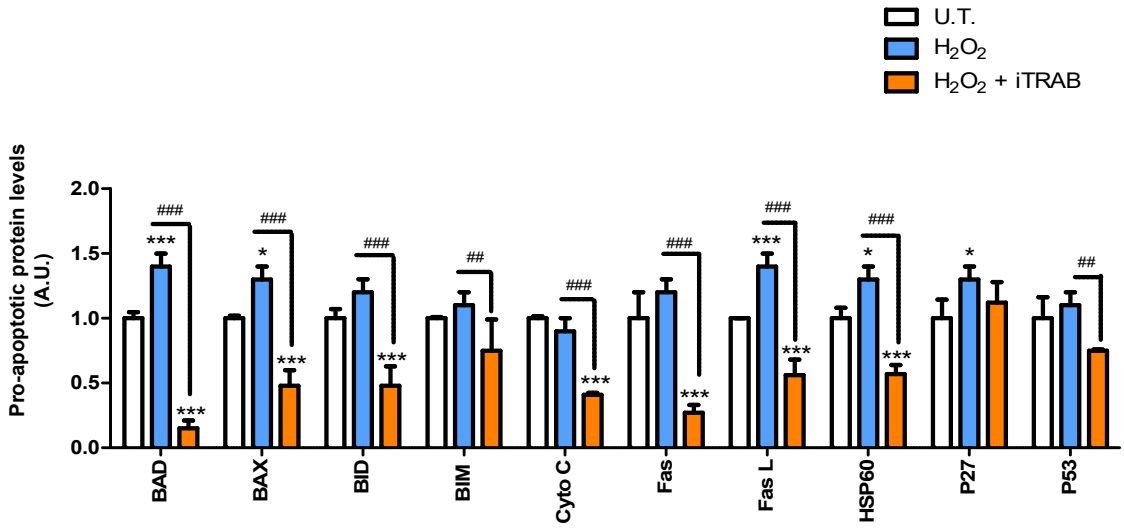

Fig.19. Apoptosis array. Analysis of pro - apoptotic protein in 3D-HTMCs cultured in dynamic condition. In the graphs only the analysis of the markers significantly modulated were reported. Twelve individual models were arrayed (six static 3D-HTMCs plus six dynamic 3D-HTMC) and per experiment the intensity of Positive Control Spot was used to normalize signal responses for comparison of results across multiple arrays. ***p<0.001; **p<0.01; *p<0.05 vs U.T. ### p<0.001; ##p<0.01; #p<0.05 vs. H2O2 + iTRAB®(Two-way ANOVA followed by Bonferroni's test).

3.8. *Preliminary findings on effects of iTRAB® on oxidative stress*

In our experimental conditions the iTRAB® administration after OS insult revealed:

- antioxidant activity (AA) as demonstrated by DCF assay, which shown a marked intracellular ROS decrease about 300%;
- counteraction of the up-regulation of TNFα, TGF-β2, IL-1 cytokines; iTRAB® up-regulated the MMP1 and MMP3 expression which are important modulators of aqueous humor outflow. A decrease of MMPs leads to an accumulation of ECM in the outflow facilities and increases the aqueous humor outflow resistance; iTRAB® reduced the pro-apoptotic protein levels.

Then, iTRAB® would seem capable to have a protective role on HTMCs against damage by OS.

Recently, it has been reported that the antioxidant properties of polyphenols could exert a plethora of health benefits in a wide range of diseases, including glaucoma through different mechanisms of action [150]. So, the antioxidant properties have gained attention as active principle of anti-glaucomatous drugs.

In particular, Saccà et al. (2019) have given evidence that iTRAB displays antioxidant protective effects on TM cells [151] thanks to the presence of the 2,3-dihydroxy-4,6-dimethoxychalcone which is an activator of the NRF2- antioxidant response element (ARE) pathway. Indeed, the NRF2 pathway activation plays a crucial role also in protecting RGCs from axonal damage [152,153]. Moreover, the iTRAB-polyunsaturated fatty acids (PUFAs) component posed by omega-3, down-regulates the inflammation cascade characteristic of glaucoma, dry eye macular degeneration [154].

Results: I*ncreased Pressure flow and iTRAB® on dynamic 3D-HTMC model.*

MTT assay and iTRAB® effects

MTT assay was carried out as a 'gold standard' to evaluate cell viability by reference to the mitochondrial compartment functionality during IOP increase exposure (**Figure. 20**). After 24 hrs of experimental treatment, the viability index of iTRAB®-treated HTMC revealed a slightly increase and it follows the trand of U.T. HTMCs at 48 and 72 hrs. However, during the experimental treatment with Live PA (IOP increase) and Live PA + iTRAB®, the mitochondrial functionality resulted impaired in the first experimental time and it restored after 72hrs of treatement with iTRAB®.

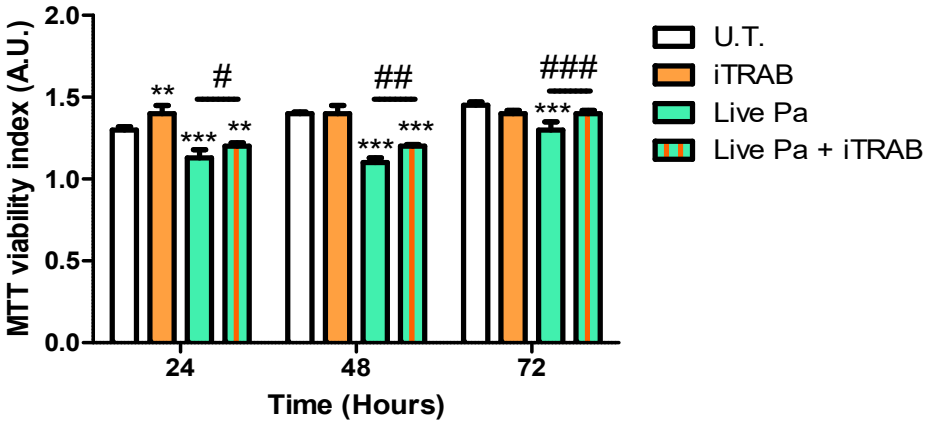

Fig.20: HTMC Viability index. Viability indices were performed by MTT Assay. Data are expressed as Arbitrary Unit (AU). Each value represent the mean ± S.D. of two separated experiments running in triplicate. ***p<0.001; **p<0.01; *p<0.05 vs U.T. ###p<0.001; ##p<0.01; #p<0.05 vs H_2O_2 + iTRAB® (Two-way ANOVA followed by Bonferroni's test)

qPCR analysis

In order to evaluate the iTRAB® antifibrotic effect after with Live PA treatment on 3D-HTMCs cultured in a dynamic manner, the cells were treated up to 72h. The gene expression levels of TGFβ, COL1A1, MYOC, α-SMA and FN1 were analyzed by qPCR (**Figure. 21**). At 72hrs Live PA-treated 3D-dynamic HTMCs showed a significantly marked up-regulation of TGFβ, COL1A1, MYOC, α-SMA and FN1 compared to untreated cultures, and their down-regulation, with gene expression levels equals to U.T. HTMCs, after the iTRAB® treatment.

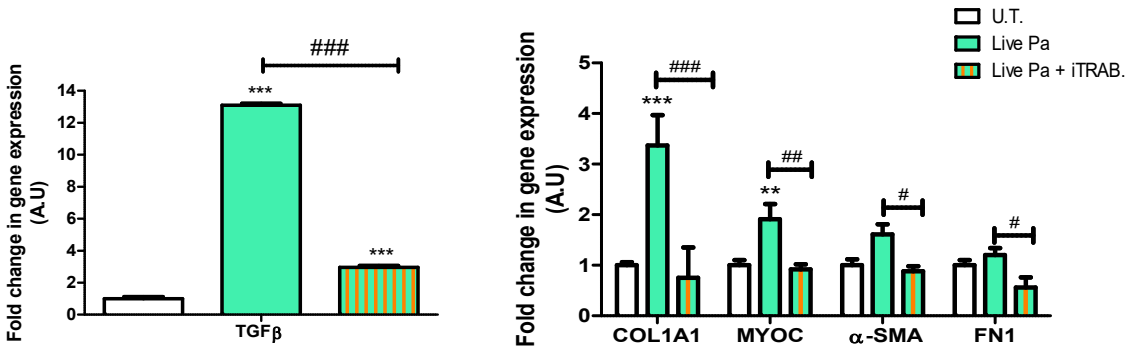

Fig.21: Gene expression. Quantitative PCR of TGF-β, COL1A1, MYOC, α-SMA and FN1 was performed at 72hrs. Data are expressed as fold-increase relative to U.T. at the same end-point and normalized to Ubiquitin housekeeping gene expression. Each bar represents the mean ± S.D. of three independent experiments performed in triplicate. ***p<0.001; **p<0.01; *p<0.05 vs U.T. ###p<0.001; ##p<0.01; #p<0.05 vs H_2O_2 + iTRAB® (Two-way ANOVA followed by Bonferroni's test)

3.9. Preliminary findings on effects of iTRAB® on increased pressure in dynamic 3D-HTMC model

The iTRAB® administration during the increased flow pressure in the cell culture chamber, revelated that this compound counteract the up-regulation both of TGF-β, COL1A1, MYOC, α-SMA and FN1, involved in ECM regulation, confirming its anti-fibrotic effect.

Furthermore, several studies have demonstrated that elevated levels of TGF-beta are found in aqueous humor and in reactive optic nerve astrocytes in patients with glaucoma. Indeed, it is hypothesized that TGF-β affects extracellular matrix homeostasis and cell contractility in the TM through interactions with other proteins, by increasing out-flow resistance. In POAG, aqueous humor outflow resistance at the trabecular meshwork (TM) leads to increased intraocular pressure and RGCs death [61].

Final Discussion

Glaucoma is identified as the second cause of blindness in the world [6], characterized by a progressive loss of RGCs, in response to a currently major risk factor that is the high IOP [155]. The TM, in adult human eye, is a major tissue involved in the conventional acqueous humor outflow pathway and its the most sensitive tissue to oxidative stress (OS) damage [130].

Therefore, the TM cellular dysfunctions such as a decrease of TM mitochondrial respiratory activity, an impairment of extracellular matrix (ECM) components and its turnover, a cellular senescence promotion and a consequent loss of its cellularity, and so on [52,156], cause an outflow resistance. Moreover, it has been hypothesized that the glaucomatous suffering of TM cells (TMCs) affects their gene and protein expression generating those molecular signals which, from anterior to posterior chamber, reach the head of the optic nerve contributing to the RGCs death [157].

The studies of TM behavior has helped to understand the pathophysiology of glaucoma: several researches has been based on animal experimentation, but the animal models present many disadvanteges due to the difference of tissue anatomy [79,80].

However, the 2D-HTMC *in vitro* model is a viable option to understand the TM behavior [148,158], but in our previous study [119] we gave evidence of the suitability of 3D-HTMC cultures for assessing a more realistic model than 2D-model. To further improve the cell environments and consequently, to create a condition “closer to in vivo”, we applied the millifluidic technique to 3D HTMC culture. In our 3D-HTMC model the HTMCs were embedded in Matrigel ®, that its consists of structural and organizational ECM components: laminin, collagen IV, heparan sulfate proteoglycan and entactin/nidogen [159], so with the Matrigel ® has been recreated *in vitro* an appropriate

microenvironment for the development of 3D-HTMC cultures, as demonstrated by Bouchemi et al., 2017 [155].

At the end of our studies, it was provided the evidence that our model maintained the tissue architecture polarity which represents an important hallmark for the tissue function maintenance found in vivo. Indeed, the cellular polarization preservation sustained a long-term viability of the cells showing the modulation of apoptosis markers and NF-kB protein levels in favor of an efficient adaptive response over time to OS-damage [160] with the trigger of the inflammation cascade instead of cell death (figure 7-8 chapter 1.2). Moreover, in a more suitable habitat the cells into dialogue with each other, by promoting cell survival and proliferation in a more realistic manner even after stimuli, such as oxidative stress.

Therefore, in our study the dynamic 3D-HTMC model turns out to be a useful tool to identify key events of glaucoma damage onset, and its long term complications, by mimicking tissue- cross talk with other tissue, joining different modeles/chambers in series. In this manner, it is possible analyze step-by-step the stage of cell damage which underlie glaucoma and its adverse outcomes.

In conclusion, to validate our dynamic 3D-HTMC model we have tested the protective effect of the iTRAB® after the OS condition and the increase of culture chamber pressure.

So, regarding iTRAB activity on 3D HTMC damaged by OS, has been shown a very significant difference in intracellular ROS production after 4hrs of experimental conditions, confirming its anti-oxidative role. The anti-inflammatory and anti-fibrotic effects of iTRAB were demonstrated by the significant reduction in IL-α, TNF-α and TGF-β cytokine profile, compared to 3D HTMC treated only by oxidative stress condition. Moreover, the iTRAB ability in remodeling the trabecular meshwork extracellular matrix composition to maintain a stable outflow resistance, was explained by the MMP1 and

MMP3 up-regulation [161]. At last, the iTRAB anti-apoptotic effect has been proven by apoptosis array which shown a marked difference in pro-apoptotic protein levels, compared both untreated 3D HTMC and 3D HTMC treated only by oxidative stress.

These results are in line with experimental evidence which highlighted the protective role of polyphenols [162].

The iTRAB was effective also against the mechanical stretch induced by the increase of culture chamber pressure. Indeed, the gene down-regulation of TGf-β and several genes involved in ECM turnover, confirmed its anti-fibrotic effect.

So, we can conclude that our in vitro advanced 3D model is useful to increase the iTRAB intracellular bioavailability in a physiological and safe manner and to study its therapeutical properties on damaged TM cells.

References

1. https://il-corpoumano.it/2730-2/.

2. Izzotti A, Bagnis A, Saccà SC. The role of oxidative stress in glaucoma. Mutat Res Mutat Res. 2006;612: 105–114. doi:10.1016/j.mrrev.2005.11.001

3. Weinreb RN, Aung T, Medeiros FA. The Pathophysiology and Treatment of Glaucoma: A Review. JAMA. 2014;311: 1901. doi:10.1001/jama.2014.3192

4. Vranka JA, Kelley MJ, Acott TS, Keller KE. Extracellular matrix in the trabecular meshwork: Intraocular pressure regulation and dysregulation in glaucoma. Exp Eye Res. 2015;133: 112–125. doi:10.1016/j.exer.2014.07.014

5. Wey S, Amanullah S, Spaeth GL, Ustaoglu M, Rahmatnejad K, Katz LJ. Is primary open-angle glaucoma an ocular manifestation of systemic disease? Graefes Arch Clin Exp Ophthalmol. 2019 [cited 18 Jan 2019]. doi:10.1007/s00417-019-04239-9

6. Quigley HA. Open-Angle Glaucoma. N Engl J Med. 1993;328: 1097–1106. doi:10.1056/NEJM199304153281507

7. Mantravadi AV, Vadhar N. Glaucoma. Prim Care Clin Off Pract. 2015;42: 437–449. doi:10.1016/j.pop.2015.05.008

8. Vohra R, Tsai JC, Kolko M. The Role of Inflammation in the Pathogenesis of Glaucoma. Surv Ophthalmol. 2013;58: 311–320. doi:10.1016/j.survophthal.2012.08.010

9. Wright AF, Dhillon B. Major progress in Fuchs's corneal dystrophy. N Engl J Med. 2010;363: 1072–1075. doi:10.1056/NEJMe1007495

10. Müller LJ, Marfurt CF, Kruse F, Tervo TMT. Corneal nerves: structure, contents and function. Exp Eye Res. 2003;76: 521–542. doi:10.1016/S0014-4835(03)00050-2

11. DelMonte DW, Kim T. Anatomy and physiology of the cornea. J Cataract Refract Surg. 2011;37: 588–598. doi:10.1016/j.jcrs.2010.12.037

12. Daniels JT, Dart JK, Tuft SJ, Khaw PT. Corneal stem cells in review. Wound Repair Regen. 2001;9: 483–494.

13. Majo F, Rochat A, Nicolas M, Jaoudé GA, Barrandon Y. Oligopotent stem cells are distributed throughout the mammalian ocular surface. Nature. 2008;456: 250.

14. Maurice DM. The transparency of the corneal stroma. Vision Res. 1970;10: 107–108. doi:10.1016/0042-6989(70)90068-4

15. Johnson DH. The Ultrastructure of Descemet's Membrane: I. Changes With Age in Normal Corneas. Arch Ophthalmol. 1982;100: 1942. doi:10.1001/archopht.1982.01030040922011

16. Willoughby CE, Ponzin D, Ferrari S, Lobo A, Landau K, Omidi Y. Anatomy and physiology of the human eye: effects of mucopolysaccharidoses disease on structure and function – a review. Clin Experiment Ophthalmol. 2010;38: 2–11. doi:10.1111/j.1442-9071.2010.02363.x

17. medtextfree. Chapter 100 – Retinal Pigment Epithelium. In: Free Medical Textbook [Internet]. 29 Dec 2010 [cited 23 Sep 2019]. Available: https://medtextfree.wordpress.com/2010/12/29/chapter-100-retinal-pigment-epithelium/

18. Miller NR, Walsh FB, Hoyt WF. Walsh and Hoyt's Clinical Neuro-ophthalmology. Lippincott Williams & Wilkins; 2005.

19. Foulds WS. Do we need a retinal pigment epithelium (or choroid) for the maintenance of retinal apposition? Br J Ophthalmol. 1985;69: 237–239. doi:10.1136/bjo.69.4.237

20. Grierson I, Hiscott P, Hogg P, Robey H, Mazure A, Larkin G. Development, repair and regeneration of the retinal pigment epithelium. Eye. 1994;8: 255–262. doi:10.1038/eye.1994.54

21. Civan MM, Macknight ADC. The ins and outs of aqueous humour secretion. Exp Eye Res. 2004;78: 625–631. doi:10.1016/j.exer.2003.09.021

22. Alm A, Nilsson SFE. Uveoscleral outflow – A review. Exp Eye Res. 2009;88: 760–768. doi:10.1016/j.exer.2008.12.012

23. Bill A. Uveoscleral drainage of aqueous humor: physiology and pharmacology. Prog Clin Biol Res. 1989;312: 417–427.

24. Tamm ER. The trabecular meshwork outflow pathways: structural and functional aspects. Exp Eye Res. 2009;88: 648–655. doi:10.1016/j.exer.2009.02.007

25. Tamm ER. The trabecular meshwork outflow pathways: Structural and functional aspects. Exp Eye Res. 2009;88: 648–655. doi:10.1016/j.exer.2009.02.007

26. Marshall GE, Konstas AG, Lee WR. Immunogold localization of type IV collagen and laminin in the aging human outflow system. Exp Eye Res. 1990;51: 691–699. doi:10.1016/0014-4835(90)90054-X

27. Marshall GE, Konstas AGP, Lee WR. Immunogold Ultrastructural Localization of Collagens in the Aged Human Outflow System. Ophthalmology. 1991;98: 692–700. doi:10.1016/S0161-6420(91)32232-2

28. Overby DR, Stamer WD, Johnson M. The changing paradigm of outflow resistance generation: Towards synergistic models of the JCT and inner wall endothelium. Exp Eye Res. 2009;88: 656–670. doi:10.1016/j.exer.2008.11.033

29. Tripathi RC. Comparative physiology and anatomy of the aqueous outflow pathwa. The eye. 1974;5: 163–336.

30. Tripathi BJ, Tripathi RC. Neural Crest Origin of Human Trabecular Meshwork and Its Implications for the Pathogenesis of Glaucoma. Am J Ophthalmol. 1989;107: 583–590. doi:10.1016/0002-9394(89)90253-5

31. Epstein DL, Freddo TF, Anderson PJ, Patterson MM, Bassett-Chu S. Experimental obstruction to aqueous outflow by pigment particles in living monkeys. Invest Ophthalmol Vis Sci. 1986;27: 387–395.

32. Keller KE, Aga M, Bradley JM, Kelley MJ, Acott TS. Extracellular matrix turnover and outflow resistance. Exp Eye Res. 2009;88: 676–682. doi:10.1016/j.exer.2008.11.023

33. Tian B, Gabelt BT, Geiger B, Kaufman PL. The role of the actomyosin system in regulating trabecular fluid outflow. Exp Eye Res. 2009;88: 713–717. doi:10.1016/j.exer.2008.08.008

34. Shuman MA, Polansky JR, Merkel C, Alvarado JA. Tissue plasminogen activator in cultured human trabecular meshwork cells. Predominance of enzyme over plasminogen activator inhibitor. Invest Ophthalmol Vis Sci. 1988;29: 401–405.

35. Shifera AS, Trivedi S, Chau P, Bonnemaison LH, Iguchi R, Alvarado JA. Constitutive secretion of chemokines by cultured human trabecular meshwork cells. Exp Eye Res. 2010;91: 42–47. doi:10.1016/j.exer.2010.04.001

36. Tripathi BJ, Tripathi RC, Wong P, Raja S. Expression of HLA by the human trabecular meshwork and corneal endothelium. Exp Eye Res. 1990;51: 269–276. doi:10.1016/0014-4835(90)90023-N

37. Bradley JMB, Anderssohn AM, Colvis CM, Parshley DE, Zhu X, Ruddat MS, et al. Mediation of Laser Trabeculoplasty–Induced Matrix Metalloproteinase Expression by IL-1β and TNFα. Invest Ophthalmol Vis Sci. 2000;41: 422–430.

38. Nucci C, Russo R, Martucci A, Giannini C, Garaci F, Floris R, et al. New strategies for neuroprotection in glaucoma, a disease that affects the central nervous system. Eur J Pharmacol. 2016;787: 119–126. doi:10.1016/j.ejphar.2016.04.030

39. Janssen SF, Gorgels TGMF, Ramdas WD, Klaver CCW, van Duijn CM, Jansonius NM, et al. The vast complexity of primary open angle glaucoma: Disease genes, risks, molecular mechanisms and pathobiology. Prog Retin Eye Res. 2013;37: 31–67. doi:10.1016/j.preteyeres.2013.09.001

40. Liu Y, Allingham RR. Major review: Molecular genetics of primary open-angle glaucoma. Exp Eye Res. 2017;160: 62–84. doi:10.1016/j.exer.2017.05.002

41. McMonnies CW. Glaucoma history and risk factors. J Optom. 2017;10: 71–78. doi:10.1016/j.optom.2016.02.003

42. Gupta D, Chen PP. Glaucoma. Am Fam Physician. 2016;93: 668–674.

43. Miller M, Fingert J, Bettis D. Genetics and genetic testing for glaucoma. Curr Opin Ophthalmol. 2017;28: 133–138. doi:10.1097/ICU.0000000000000344

44. Swarup G, Sayyad Z. Altered Functions and Interactions of Glaucoma-Associated Mutants of Optineurin. Front Immunol. 2018;9: 1287. doi:10.3389/fimmu.2018.01287

45. DeLuca AP, Alward WLM, Liebmann J, Ritch R, Kawase K, Kwon YH, et al. Genomic Organization of TBK1 Copy Number Variations in Glaucoma Patients. J Glaucoma. 2017;26: 1063–1067. doi:10.1097/IJG.0000000000000792

46. Neetens A. A neuro-ophthalmologist looks at primary open angle glaucoma and soft glaucoma (POAG). Neuro-Ophthalmol. 1994;14: 53–59. doi:10.3109/01658109409019487

47. Pinazo-Durán MD, Zanón-Moreno V, Gallego-Pinazo R, García-Medina JJ. Chapter 6 - Oxidative stress and mitochondrial failure in the pathogenesis of glaucoma neurodegeneration. In: Bagetta G, Nucci C, editors. Progress in Brain Research. Elsevier; 2015. pp. 127–153. doi:10.1016/bs.pbr.2015.06.001

48. Russo R, Varano GP, Adornetto A, Nucci C, Corasaniti MT, Bagetta G, et al. Retinal ganglion cell death in glaucoma: Exploring the role of neuroinflammation. Eur J Pharmacol. 2016;787: 134–142. doi:10.1016/j.ejphar.2016.03.064

49. Zhao L, Chen G, Li J, Fu Y, Mavlyutov TA, Yao A, et al. An intraocular drug delivery system using targeted nanocarriers attenuates retinal ganglion cell degeneration. J Controlled Release. 2017;247: 153–166. doi:10.1016/j.jconrel.2016.12.038

50. Flammer J, Haefliger IO, Orgül S, Resink T. Vascular dysregulation: a principal risk factor for glaucomatous damage? J Glaucoma. 1999;8: 212–219.

51. Zhao J, Wang S, Zhong W, Yang B, Sun L, Zheng Y. Oxidative stress in the trabecular meshwork (Review). Int J Mol Med. 2016;38: 995–1002. doi:10.3892/ijmm.2016.2714

52. Kim SH, Kim H. Inhibitory Effect of Astaxanthin on Oxidative Stress-Induced Mitochondrial Dysfunction-A Mini-Review. Nutrients. 2018;10: 1137. doi:10.3390/nu10091137

53. Keller KE, Bradley JM, Vranka JA, Acott TS. Segmental Versican Expression in the Trabecular Meshwork and Involvement in Outflow Facility. Investig Opthalmology Vis Sci. 2011;52: 5049. doi:10.1167/iovs.10-6948

54. Stamer WD, Clark AF. The many faces of the trabecular meshwork cell. Exp Eye Res. 2017;158: 112–123.

55. Acott TS, Kelley MJ, Keller KE, Vranka JA, Abu-Hassan DW, Li X, et al. Intraocular Pressure Homeostasis: Maintaining Balance in a High-Pressure Environment. J Ocul Pharmacol Ther. 2014;30: 94–101. doi:10.1089/jop.2013.0185

56. Acott TS, Kelley MJ. Extracellular matrix in the trabecular meshwork. Exp Eye Res. 2008;86: 543–561. doi:10.1016/j.exer.2008.01.013

57. Lütjen-Drecoll E. Functional morphology of the trabecular meshwork in primate eyes. Prog Retin Eye Res. 1999;18: 91–119. doi:10.1016/S1350-9462(98)00011-1

58. Rasmussen CA, Kaufman PL, Duehr PA, Bárány EH. The trabecular meshwork in normal eyes and in exfoliation glaucoma. J Glaucoma. 2014;23: S15–S19. doi:10.1097/IJG.0000000000000106

59. Scott JE. Secondary Structures in Hyaluronan Solutions: Chemical and Biological Implications. Ciba Foundation Symposium 143 - The Biology of Hyaluronan. John Wiley & Sons, Ltd; 2007. pp. 6–20. doi:10.1002/9780470513774.ch2

60. Ruoslahti E, Yamaguchi Y. Proteoglycans as modulators of growth factor activities. Cell. 1991;64: 867–869. doi:10.1016/0092-8674(91)90308-L

61. Tripathi RC, Li J, Chan WA, Tripathi BJ. Aqueous Humor in Glaucomatous Eyes Contains an Increased Level of TGF-β2. Exp Eye Res. 1994;59: 723–728. doi:10.1006/exer.1994.1158

62. Chatterjee A, Villarreal G, Rhee DJ. Matricellular Proteins in the Trabecular Meshwork: Review and Update. J Ocul Pharmacol Ther. 2014;30: 447–463. doi:10.1089/jop.2014.0013

63. Yanagi M, Kawasaki R, Wang JJ, Wong TY, Crowston J, Kiuchi Y. Vascular risk factors in glaucoma: a review. Clin Experiment Ophthalmol. 2011;39: 252–258. doi:10.1111/j.1442-9071.2010.02455.x

64. Friedlander AH, Graves LL, Chang TI, Kawakami KK, Lee UK, Grabich SC, et al. Prevalence of primary open-angle glaucoma among patients with obstructive sleep apnea. Oral Surg Oral Med Oral Pathol Oral Radiol. 2018;126: 226–230. doi:10.1016/j.oooo.2018.01.021

65. Zhao D, Cho J, Kim MH, Friedman D, Guallar E. Diabetes, Glucose Metabolism, and Glaucoma: The 2005–2008 National Health and Nutrition Examination Survey. PLOS ONE. 2014;9: e112460. doi:10.1371/journal.pone.0112460

66. Križaj D. What is glaucoma? In: Kolb H, Fernandez E, Nelson R, editors. Webvision: The Organization of the Retina and Visual System. Salt Lake City (UT): University of Utah Health Sciences Center; 1995. Available: http://www.ncbi.nlm.nih.gov/books/NBK543075/

67. fundus e fovea].Available: https://www.google.com/search?q=fundus+e+fovea&sxsrf=ACYBGNT8vqvl1aCNMFqWkiCh09tsa5m7zw:1569590466898&tbm=isch&source=iu&ictx=1&fir=XqJmLWSocJ8tuM%253A%252CVGgE1haYrn3pWM%252C_&vet=1&usg=AI4_-kRNLhoatu0YMQqanLFCK80Q9CGWnQ&sa=X&ved=2ahUKEwjLneORjPHkAhWQDewKHbM5CKEQ9QEwAnoECAYQCQ#imgrc=o7pEk92FEqcpCM:&vet=1

68. Hagiwara Y, Koh JEW, Tan JH, Bhandary SV, Laude A, Ciaccio EJ, et al. Computer-aided diagnosis of glaucoma using fundus images: A review. Comput Methods Programs Biomed. 2018;165: 1–12. doi:10.1016/j.cmpb.2018.07.012

69. de Moraes CG, Liebmann JM, Medeiros FA, Weinreb RN. Management of advanced glaucoma: Characterization and monitoring. Surv Ophthalmol. 2016;61: 597–615. doi:10.1016/j.survophthal.2016.03.006

70. McMonnies CW. Glaucoma history and risk factors. J Optom. 2017;10: 71–78. doi:10.1016/j.optom.2016.02.003

71. Weinreb RN, Aung T, Medeiros FA. The Pathophysiology and Treatment of Glaucoma. JAMA. 2014;311: 1901–1911. doi:10.1001/jama.2014.3192

72. Graf BA, Milbury PE, Blumberg JB. Flavonols, Flavones, Flavanones, and Human Health: Epidemiological Evidence. J Med Food. 2005;8: 281–290. doi:10.1089/jmf.2005.8.281

73. Arts IC, Hollman PC. Polyphenols and disease risk in epidemiologic studies. Am J Clin Nutr. 2005;81: 317S-325S. doi:10.1093/ajcn/81.1.317S

74. Protection of trabecular meshwork cells by eyedrops containing high concentration of polyphenols. [cited 19 Sep 2019]. Available: https://oatext.com/protection-of-trabecular-meshwork-cells-by-eyedrops-containing-high-concentration-of-polyphenols.php

75. Secades JJ. Citicoline: pharmacological and clinical review, 2016 update. Rev Neurol. 2016;63: S1–S73.

76. Chang EE, Goldberg JL. Glaucoma 2.0: Neuroprotection, Neuroregeneration, Neuroenhancement. Ophthalmology. 2012;119: 979–986. doi:10.1016/j.ophtha.2011.11.003

77. Roberti G, Tanga L, Parisi V, Sampalmieri M, Centofanti M, Manni G. A preliminary study of the neuroprotective role of citicoline eye drops in glaucomatous optic neuropathy. Indian J Ophthalmol. 2014;62: 549–553. doi:10.4103/0301-4738.133484

78. Struebing FL, Geisert EE. Chapter Twenty-One - What Animal Models Can Tell Us About Glaucoma. In: Hejtmancik JF, Nickerson JM, editors. Progress in Molecular Biology and Translational Science. Academic Press; 2015. pp. 365–380. doi:10.1016/bs.pmbts.2015.06.003

79. Quigley HA. Use of Animal Models and Techniques in Glaucoma Research: Introduction. In: Jakobs TC, editor. Glaucoma: Methods and Protocols. New York, NY: Springer New York; 2018. pp. 1–10. doi:10.1007/978-1-4939-7407-8_1

80. A. Bouhenni R, Dunmire J, Sewell A, Edward DP. Animal Models of Glaucoma. J Biomed Biotechnol. 2012;2012. doi:10.1155/2012/692609

81. Aires ID, Ambrósio AF, Santiago AR. Modeling Human Glaucoma: Lessons from the in vitro Models. Ophthalmic Res. 2017;57: 77–86. doi:10.1159/000448480

82. Langley GR, Adcock IM, Busquet F, Crofton KM, Csernok E, Giese C, et al. Towards a 21st-century roadmap for biomedical research and drug discovery: consensus report and recommendations. Drug Discov Today. 2017;22: 327–339. doi:10.1016/j.drudis.2016.10.011

83. Gaasterland D, Kupfer C. Reports: Experimental Glaucoma in the Rhesus Monkey. Invest Ophthalmol Vis Sci. 1974;13: 455–457.

84. Ishikawa M, Yoshitomi T, Zorumski CF, Izumi Y. Experimentally Induced Mammalian Models of Glaucoma. In: BioMed Research International [Internet]. 2015 [cited 18 Jan 2019]. doi:10.1155/2015/281214

85. Aihara M, Lindsey JD, Weinreb RN. Experimental Mouse Ocular Hypertension: Establishment of the Model. Invest Ophthalmol Vis Sci. 2003;44: 4314–4320. doi:10.1167/iovs.03-0137

86. Levkovitch-Verbin H, Quigley HA, Martin KRG, Valenta D, Baumrind LA, Pease ME. Translimbal Laser Photocoagulation to the Trabecular Meshwork as a Model of Glaucoma in Rats. Invest Ophthalmol Vis Sci. 2002;43: 402–410.

87. Kalvin NH. Experimental Glaucoma in Monkeys: I. Relationship Between Intraocular Pressure and Cupping of the Optic Disc and Cavernous Atrophy of the Optic Nerve. Arch Ophthalmol. 1966;76: 82. doi:10.1001/archopht.1966.03850010084017

88. Steinhart MR, Cone FE, Nguyen C, Nguyen TD, Pease ME, Puk O, et al. Mice with an induced mutation in collagen 8A2 develop larger eyes and are resistant to retinal ganglion cell damage in an experimental glaucoma model. Mol Vis. 2012;18: 1093–1106.

89. Ngumah QC, Buchthal SD, Dacheux RF. Longitudinal non-invasive proton NMR spectroscopy measurement of vitreous lactate in a rabbit model of ocular hypertension. Exp Eye Res. 2006;83: 390–400. doi:10.1016/j.exer.2006.01.015

90. Quigley HA, Addicks EM. Chronic experimental glaucoma in primates. I. Production of elevated intraocular pressure by anterior chamber injection of autologous ghost red blood cells. Invest Ophthalmol Vis Sci. 1980;19: 126–136.

91. Grozdanic SD, Betts DM, Sakaguchi DS, Kwon YH, Kardon RH, Sonea IM. Temporary elevation of the intraocular pressure by cauterization of vortex and episcleral veins in rats causes functional deficits in the retina and optic nerve. Exp Eye Res. 2003;77: 27–33. doi:10.1016/S0014-4835(03)00089-7

92. Yu S, Tanabe T, Yoshimura N. A rat model of glaucoma induced by episcleral vein ligation. Exp Eye Res. 2006;83: 758–770. doi:10.1016/j.exer.2006.03.014

93. Shareef SR, Garcia-Valenzuela E, Salierno A, Walsh J, Sharma SC. Chronic ocular hypertension following episcleral venous occlusion in rats. Exp Eye Res. 1995;61: 379–382. doi:10.1016/s0014-4835(05)80131-9

94. Kipfer-Kauer A, McKinnon SJ, Frueh BE, Goldblum D. Distribution of Amyloid Precursor Protein and Amyloid-β in Ocular Hypertensive C57BL/6 Mouse Eyes. Curr Eye Res. 2010;35: 828–834. doi:10.3109/02713683.2010.494240

95. Rudzinski M, Saragovi HU. Glaucoma: Validated and Facile In Vivo Experimental Models of a Chronic Neurodegenerative Disease for Drug Development. 2005 [cited 26 Sep 2019]. doi:info:doi/10.2174/1568015053202796

96. Johnson TV, Tomarev SI. Rodent models of glaucoma. Brain Res Bull. 2010;81: 349–358. doi:10.1016/j.brainresbull.2009.04.004

97. Evangelho K, Mogilevskaya M, Losada-Barragan M, Vargas-Sanchez JK. Pathophysiology of primary open-angle glaucoma from a neuroinflammatory and neurotoxicity perspective: a review of the literature. Int Ophthalmol. 2019;39: 259–271. doi:10.1007/s10792-017-0795-9

98. Brancato V, Gioiella F, Imparato G, Guarnieri D, Urciuolo F, Netti PA. 3D breast cancer microtissue reveals the role of tumor microenvironment on the transport and efficacy of free-doxorubicin in vitro. Acta Biomater. 2018;75: 200–212. doi:10.1016/j.actbio.2018.05.055

99. Vernazza S, Tirendi S, Scarfì S, Passalacqua M, Oddone F, Traverso CE, et al. 2D- and 3D-cultures of human trabecular meshwork cells: A preliminary assessment of an in vitro model for glaucoma study. PLOS ONE. 2019;14: e0221942. doi:10.1371/journal.pone.0221942

100. Berger E, Magliaro C, Paczia N, Monzel AS, Antony P, Linster CL, et al. Millifluidic culture improves human midbrain organoid vitality and differentiation. Lab Chip. 2018;18: 3172–3183. doi:10.1039/C8LC00206A

101. Giusti S, Sbrana T, La Marca M, Di Patria V, Martinucci V, Tirella A, et al. A novel dual-flow bioreactor simulates increased fluorescein permeability in epithelial tissue barriers. Biotechnol J. 2014;9: 1175–1184. doi:10.1002/biot.201400004

102. Tokuda S, Kim YH, Matsumoto H, Muro S, Hirai T, Mishima M, et al. Effects of Hydrostatic Pressure on Carcinogenic Properties of Epithelia. PloS One. 2015;10: e0145522. doi:10.1371/journal.pone.0145522

103. Kao Y-C, Lee C-H, Kuo P-L. Increased hydrostatic pressure enhances motility of lung cancer cells. Conf Proc Annu Int Conf IEEE Eng Med Biol Soc IEEE Eng Med Biol Soc Annu Conf. 2014;2014: 2928–2931. doi:10.1109/EMBC.2014.6944236

104. Rao F, Yang R-Q, Chen X-S, Xu J-S, Fu H-M, Su H, et al. PPARγ ligands decrease hydrostatic pressure-induced platelet aggregation and proinflammatory activity. PloS One. 2014;9: e89654. doi:10.1371/journal.pone.0089654

105. Kaarniranta K, Elo M, Sironen R, Lammi MJ, Goldring MB, Eriksson JE, et al. Hsp70 accumulation in chondrocytic cells exposed to high continuous hydrostatic pressure coincides with mRNA stabilization rather than transcriptional activation. Proc Natl Acad Sci U S A. 1998;95: 2319–2324. doi:10.1073/pnas.95.5.2319

106. Yang JL, Neufeld AH, Zorn MB, Hernandez MR. Collagen type I mRNA levels in cultured human lamina cribrosa cells: effects of elevated hydrostatic pressure. Exp Eye Res. 1993;56: 567–574. doi:10.1006/exer.1993.1070

107. Obazawa M, Mashima Y, Sanuki N, Noda S, Kudoh J, Shimizu N, et al. Analysis of porcine optineurin and myocilin expression in trabecular meshwork cells and astrocytes from optic nerve head. Invest Ophthalmol Vis Sci. 2004;45: 2652–2659. doi:10.1167/iovs.03-0572

108. Keller KE, Bhattacharya SK, Borrás T, Brunner TM, Chansangpetch S, Clark AF, et al. Consensus recommendations for trabecular meshwork cell isolation,

characterization and culture. Exp Eye Res. 2018;171: 164–173. doi:10.1016/j.exer.2018.03.001

109. Keller KE, Bhattacharya SK, Borrás T, Brunner TM, Chansangpetch S, Clark AF, et al. Consensus recommendations for trabecular meshwork cell isolation, characterization and culture. Exp Eye Res. 2018;171: 164–173. doi:10.1016/j.exer.2018.03.001

110. Poehlmann A, Reissig K, Schönfeld P, Walluscheck D, Schinlauer A, Hartig R, et al. Repeated H2O2 exposure drives cell cycle progression in an in vitro model of ulcerative colitis. J Cell Mol Med. 2013;17: 1619–1631. doi:10.1111/jcmm.12150

111. Wang H, Joseph JA. Quantifying cellular oxidative stress by dichlorofluorescein assay using microplate reader11Mention of a trade name, proprietary product, or specific equipment does not constitute a guarantee by the United States Department of Agriculture and does not imply its approval to the exclusion of other products that may be suitable. Free Radic Biol Med. 1999;27: 612–616. doi:10.1016/S0891-5849(99)00107-0

112. Mosmann T. Rapid colorimetric assay for cellular growth and survival: Application to proliferation and cytotoxicity assays. J Immunol Methods. 1983;65: 55–63. doi:10.1016/0022-1759(83)90303-4

113. Aarskog N, Vedeler C. Real-time quantitative polymerase chain reaction. Hum Genet. 2000;107: 494–498. doi:10.1007/s004390000399

114. Vandesompele J, De Preter K, Pattyn F, Poppe B, Van Roy N, De Paepe A, et al. Accurate normalization of real-time quantitative RT-PCR data by geometric averaging of multiple internal control genes. Genome Biol. 2002;3: research0034.1. doi:10.1186/gb-2002-3-7-research0034

115. Regier MC, Montanez-Sauri SI, Schwartz MP, Murphy WL, Beebe DJ, Sung KE. The Influence of Biomaterials on Cytokine Production in 3D Cultures. Biomacromolecules. 2017;18: 709–718. doi:10.1021/acs.biomac.6b01469

116. Duval K, Grover H, Han L-H, Mou Y, Pegoraro AF, Fredberg J, et al. Modeling Physiological Events in 2D vs. 3D Cell Culture. Physiology. 2017;32: 266–277. doi:10.1152/physiol.00036.2016

117. Edmondson R, Broglie JJ, Adcock AF, Yang L. Three-Dimensional Cell Culture Systems and Their Applications in Drug Discovery and Cell-Based Biosensors. ASSAY Drug Dev Technol. 2014;12: 207–218. doi:10.1089/adt.2014.573

118. Bhadriraju K, Chen CS. Engineering cellular microenvironments to improve cell-based drug testing. Drug Discov Today. 2002;7: 612–620. doi:10.1016/s1359-6446(02)02273-0

119. Vernazza S, Tirendi S, Scarfì S, Passalacqua M, Oddone F, Traverso CE, et al. 2D- and 3D-cultures of human trabecular meshwork cells: A preliminary assessment of an in vitro model for glaucoma study. PLOS ONE. 2019;14: e0221942-. doi:10.1371/journal.pone.0221942

120. Huh D, Hamilton GA, Ingber DE. From 3D cell culture to organs-on-chips. Trends Cell Biol. 2011;21: 745–754. doi:10.1016/j.tcb.2011.09.005

121. Jeyasuria P, Subedi K, Suresh A, Condon JC. Elevated Levels of Uterine Anti-Apoptotic Signaling May Activate NFKB and Potentially Confer Resistance to Caspase 3-Mediated Apoptotic Cell Death During Pregnancy in Mice1. Biol Reprod. 2011;85: 417–424. doi:10.1095/biolreprod.111.091652

122. Gibson L, Holmgreen SP, Huang DC, Bernard O, Copeland NG, Jenkins NA, et al. bcl-w, a novel member of the bcl-2 family, promotes cell survival. Oncogene. 1996;13: 665–675.

123. Raja Singh P, Arunkumar R, Sivakamasundari V, Sharmila G, Elumalai P, Suganthapriya E, et al. Anti-proliferative and apoptosis inducing effect of nimbolide by altering molecules involved in apoptosis and IGF signalling via PI3K/Akt in prostate cancer (PC-3) cell line: EFFECT OF NIMBOLIDE IN PC-3 CELL LINE. Cell Biochem Funct. 2014;32: 217–228. doi:10.1002/cbf.2993

124. Capoluongo E. Insulin-Like Growth Factor System and Sporadic Malignant Melanoma. Am J Pathol. 2011;178: 26–31. doi:10.1016/j.ajpath.2010.11.004

125. Dunn SE, Hardman RA, Kari FW, Barrett JC. Insulin-like Growth Factor 1 (IGF-1) Alters Drug Sensitivity of HBL100 Human Breast Cancer Cells by Inhibition of Apoptosis Induced by Diverse Anticancer Drugs. Cancer Res. 1997;57: 2687–2693.

126. Karin M. Nuclear factor-κB in cancer development and progression. Nature. 2006;441: 431–436. doi:10.1038/nature04870

127. Zambrano S, Toma ID, Piffer A, Bianchi ME, Agresti A. NF-kB oscillations translate into functionally related patterns of gene expression. : 38.

128. Ucciferri N, Sbrana T, Ahluwalia A. Allometric Scaling and Cell Ratios in Multi-Organ in vitro Models of Human Metabolism. Front Bioeng Biotechnol. 2014;2. doi:10.3389/fbioe.2014.00074

129. Kaczara P, Sarna T, Burke JM. Dynamics of H2O2 availability to ARPE-19 cultures in models of oxidative stress. Free Radic Biol Med. 2010;48: 1064–1070. doi:10.1016/j.freeradbiomed.2010.01.022

130. Saccà SC, Gandolfi S, Bagnis A, Manni G, Damonte G, Traverso CE, et al. The Outflow Pathway: A Tissue With Morphological and Functional Unity. J Cell Physiol. 2016;231: 1876–1893. doi:10.1002/jcp.25305

131. Pulliero A, Seydel A, Camoirano A, Saccà SC, Sandri M, Izzotti A. Oxidative Damage and Autophagy in the Human Trabecular Meshwork as Related with Ageing. Reddy H, editor. PLoS ONE. 2014;9: e98106. doi:10.1371/journal.pone.0098106

132. Lv X-X, Liu S-S, Hu Z-W. Autophagy-inducing natural compounds: a treasure resource for developing therapeutics against tissue fibrosis. J Asian Nat Prod Res. 2017;19: 101–108. doi:10.1080/10286020.2017.1279151

133. Taurone S, Ripandelli G, Pacella E, Bianchi E, Plateroti AM, De Vito S, et al. Potential regulatory molecules in the human trabecular meshwork of patients with

glaucoma: Immunohistochemical profile of a number of inflammatory cytokines. Mol Med Rep. 2015;11: 1384–1390. doi:10.3892/mmr.2014.2772

134. Micheal S, Yousaf S, Khan MI, Akhtar F, Islam F, Khan WA, et al. Polymorphisms in matrix metalloproteinases MMP1 and MMP9 are associated with primary open-angle and angle closure glaucoma in a Pakistani population. Mol Vis. 2013;19: 441–447.

135. Singh D, Srivastava SK, Chaudhuri TK, Upadhyay G. Multifaceted role of matrix metalloproteinases (MMPs). Front Mol Biosci. 2015;2. doi:10.3389/fmolb.2015.00019

136. Acott TS, Kelley MJ. Extracellular matrix in the trabecular meshwork. Exp Eye Res. 2008;86: 543–561. doi:10.1016/j.exer.2008.01.013

137. Wang N, Chintala SK, Fini ME, Schuman JS. Activation of a tissue-specific stress response in the aqueous outflow pathway of the eye defines the glaucoma disease phenotype. Nat Med. 2001;7: 304. doi:10.1038/85446

138. Zahir N, Weaver VM. Death in the third dimension: apoptosis regulation and tissue architecture. Curr Opin Genet Dev. 2004;14: 71–80. doi:10.1016/j.gde.2003.12.005

139. Elmore S. Apoptosis: a review of programmed cell death. Toxicol Pathol. 2007;35: 495–516. doi:10.1080/01926230701320337

140. Vanamee ÉS, Faustman DL. TNFR2: A Novel Target for Cancer Immunotherapy. Trends Mol Med. 2017;23: 1037–1046. doi:10.1016/j.molmed.2017.09.007

141. Magliaro C, Rinaldo A, Ahluwalia A. Allometric Scaling of physiologically-relevant organoids. bioRxiv. 2019; 559682. doi:10.1101/559682

142. Vranka JA, Acott TS. Pressure-induced expression changes in segmental flow regions of the human trabecular meshwork. Exp Eye Res. 2017;158: 67–72.

143. Izzotti A, Bagnis A, Saccà SC. The role of oxidative stress in glaucoma. Mutat Res Mutat Res. 2006;612: 105–114. doi:10.1016/j.mrrev.2005.11.001

144. Saccà SC, Izzotti A, Rossi P, Traverso C. Glaucomatous outflow pathway and oxidative stress. Exp Eye Res. 2007;84: 389–399. doi:10.1016/j.exer.2006.10.008

145. Wang N, Chintala SK, Fini ME, Schuman JS. Activation of a tissue-specific stress response in the aqueous outflow pathway of the eye defines the glaucoma disease phenotype. Nat Med. 2001;7: 304–309. doi:10.1038/85446

146. Wei H-Y, Liu J-L, Lv B-J, Xing L, Fu S-Y. SPARC modulates expression of extracellular matrix genes in human trabecular meshwork cells. Acta Ophthalmol (Copenh). 2012;90: e138–e143.

147. Synergism of TNF and IL-1 in the Induction of Matrix Metalloproteinase-3 in Trabecular Meshwork | IOVS | ARVO Journals. [cited 22 Feb 2019]. Available: https://iovs.arvojournals.org/article.aspx?articleid=2164638

148. Rhee DJ, Haddadin RI, Kang MH, Oh D-J. Matricellular proteins in the trabecular meshwork. Exp Eye Res. 2009;88: 694–703. doi:10.1016/j.exer.2008.11.032

149. Itakura T, Peters DM, Fini ME. Glaucomatous MYOC mutations activate the IL-1/NF-κB inflammatory stress response and the glaucoma marker SELE in trabecular meshwork cells. Mol Vis. 2015;21: 1071–1084.

150. Abu-Amero K, Kondkar A, Chalam K. Resveratrol and Ophthalmic Diseases. Nutrients. 2016;8: 200. doi:10.3390/nu8040200

151. C. Sacca S, Pulliero A, La Maestra S, Geretto M, Profumo A, Ilderbayev O, et al. Protection of trabecular meshwork cells by eyedrops containing high concentration of polyphenols. New Front Ophthalmol. 2019;5. doi:10.15761/NFO.1000228

152. Sitte N, Merker K, Von Zglinicki T, Grune T, Davies KJA. Protein oxidation and degradation during cellular senescence of human BJ fibroblasts: part I—effects of proliferative senescence. FASEB J. 2000;14: 2495–2502. doi:10.1096/fj.00-0209com

153. Masaki Y, Izumi Y, Matsumura A, Akaike A, Kume T. Protective effect of Nrf2–ARE activator isolated from green perilla leaves on dopaminergic neuronal loss in a Parkinson's disease model. Eur J Pharmacol. 2017;798: 26–34. doi:10.1016/j.ejphar.2017.02.005

154. Wall R, Ross RP, Fitzgerald GF, Stanton C. Fatty acids from fish: the anti-inflammatory potential of long-chain omega-3 fatty acids. Nutr Rev. 2010;68: 280–289. doi:10.1111/j.1753-4887.2010.00287.x

155. Bouchemi M, Roubeix C, Kessal K, Riancho L, Raveu A-L, Soualmia H, et al. Effect of benzalkonium chloride on trabecular meshwork cells in a new in vitro 3D trabecular meshwork model for glaucoma. Toxicol In Vitro. 2017;41: 21–29. doi:10.1016/j.tiv.2017.02.006

156. Zhao J, Wang S, Zhong W, Yang B, Sun L, Zheng Y. Oxidative stress in the trabecular meshwork (Review). Int J Mol Med. 2016;38: 995–1002. doi:10.3892/ijmm.2016.2714

157. Saccà SC, Gandolfi S, Bagnis A, Manni G, Damonte G, Traverso CE, et al. From DNA damage to functional changes of the trabecular meshwork in aging and glaucoma. Ageing Res Rev. 2016;29: 26–41. doi:10.1016/j.arr.2016.05.012

158. Stamer DW, Roberts BC, Epstein DL, Allingham RR. Isolation of primary open-angle glaucomatous trabecular meshwork cells from whole eye tissue. Curr Eye Res. 2000;20: 347–350.

159. Kleinman HK, Martin GR. Matrigel: basement membrane matrix with biological activity. Semin Cancer Biol. 2005;15: 378–386. doi:10.1016/j.semcancer.2005.05.004

160. Zahir N, Weaver VM. Death in the third dimension: apoptosis regulation and tissue architecture. Curr Opin Genet Dev. 2004;14: 71–80. doi:10.1016/j.gde.2003.12.005

161. De Groef L, Van Hove I, Dekeyster E, Stalmans I, Moons L. MMPs in the Trabecular Meshwork: Promising Targets for Future Glaucoma Therapies? Investig Opthalmology Vis Sci. 2013;54: 7756. doi:10.1167/iovs.13-13088

162. Zhao Z, Sun T, Jiang Y, Wu L, Cai X, Sun X, et al. Photooxidative damage in retinal pigment epithelial cells via GRP78 and the protective role of grape skin polyphenols. Food Chem Toxicol. 2014;74: 216–224. doi:10.1016/j.fct.2014.10.001

PLOS ONE

RESEARCH ARTICLE

2D- and 3D-cultures of human trabecular meshwork cells: A preliminary assessment of an in vitro model for glaucoma study

Stefania Vernazza[1☯*], Sara Tirendi[2,3☯], Sonia Scarfì[3,4], Mario Passalacqua[2,3], Francesco Oddone[1], Carlo Enrico Traverso[5], Ilaria Rizzato[3,6], Anna Maria Bassi[2,3‡], Sergio Claudio Saccà[7‡]

1 IRCCS, Fondazione G.B. Bietti, Rome, Italy, **2** Department of Experimental Medicine (DIMES), University of Genoa, Genoa, Italy, **3** Inter-University Center for the Promotion of the 3Rs Principles in Teaching & Research (Centro 3R), Italy, **4** Department of Earth, Environment and Life Sciences (DISTAV), University of Genoa, Genoa, Italy, **5** Department of Neuroscience, Rehabilitation, Ophthalmology, Genetics, Maternal and Child Health (DINOGMI), University of Genoa, Genoa, Italy, **6** Department of Modern Languages and Cultures (LCM), University of Genoa, Genoa, Italy, **7** IRCCS, San Martino General Hospital, Ophthalmology Unit, Genoa, Italy

☯ These authors contributed equally to this work.
‡ These authors also contributed equally to this study.
* stefania.vernazza@yahoo.it

OPEN ACCESS

Citation: Vernazza S, Tirendi S, Scarfì S, Passalacqua M, Oddone F, Traverso CE, et al. (2019) 2D- and 3D-cultures of human trabecular meshwork cells: A preliminary assessment of an in vitro model for glaucoma study. PLoS ONE 14(9): e0221942. https://doi.org/10.1371/journal.pone.0221942

Editor: Ted S. Acott, Oregon Health and Science University, UNITED STATES

Received: May 22, 2019

Accepted: August 19, 2019

Published: September 6, 2019

Abstract

A physiologically relevant *in vitro* human-based model could be the 'gold standard' to clarify the pathological steps involved in glaucoma onset. In this regard, human 3D cultures may represent an excellent starting point to achieve this goal. Indeed, the 3D matrix allows to re-create the in vivo-like tissue architecture, maintaining its functionality and cellular behaviour, compared to the 2D model. Thus, we propose a comparison between the 2D and 3D in vitro models of human trabecular meshwork cells in terms of cellular responses after chronic stress exposure. Our results showed that 3D-cells are more sensitive to intracellular reactive oxidative specie production induced by hydrogen peroxide treatment, compared to 2D cultures. Additionally, in 3D cultures a more accurate regulation of the apoptosis trigger and cell adaptation mechanisms was detected than in 2D models. In line with these findings, the 3D-HTMC model shows the ability to better mimic the in vivo cell behaviour in adaptive responses to chronic oxidative stress than 2D.

128

Development of advancing human 3D trabecular meshwork models to assess onset of glaucoma

Sara Tirendi [1], Stefania Vernazza [1,2], Mario Passalacqua [1], Sergio Saccà [3] and Anna Maria Bassi [1,4]

[1]University of Genoa – Department of Experimental Medicine (DIMES), Genoa, Italy; [2]The G.B. Bietti Foundation for Study and Research in Ophthalmology, Genoa, Italy; [3]San Martino Polyclinic Hospital, Genoa, Italy; [4]Centro3R, Genoa, Italy

Glaucoma is a progressive optic neuropathy that leads to irreversible blindness. As known, the main causes of glaucoma onset are oxidative stress and vascular alteration, which damage trabecular meshwork (TM) status, impairing the eye's drainage system which in turn, increase intraocular pressure (IOP). Nowadays IOP is the only hallmark of disease and therapies can slow down it, without prevent blindness [1,2]. In addition, the glaucoma diagnosis occurs too late because most of screening tests are not predictive. The lack of glaucoma models human-based is the mainly limitation for drug discovery.

Therefore, the aim of this study was to develop an *in vitro* human-based model to define the key events involved in the onset of glaucoma, and its long-term complications. The model could be a useful tool to select and check targets for therapeutic drugs to prevent or treat glaucoma disease.

Firstly three different *in vitro* models of human TM cells, conventional 2D and innovative 3D-static and –biodynamic models, were assessed, to verify which better mimics the glaucoma onset.

For 3D models, TM cells were embedded into Matrigel, and dynamic condition was set up using a fluidic multi-chamber device, connected with a peristaltic pump (LiveBox1 and Live Flow, IV-Tech srl). While 2D-TM, after 7 days of standard culture conditions, showed a marked suffering, the 3D-TMs were cultured up to 15 days. The metabolic state, performed by Alamar blue assay, pointed out a better healthy state of 3Ds vs 2D. This effect was confirmed also by confocal imaging that evidenced a cellular morphology and organization more similar to physiological environment in 3D-TM.

Starting by these observations, we analyzed if the different TM-models could response otherwise to a chronic stress, mimicked by daily exposure for 2 h to 500 µM H_2O_2, with 22 h recovery phases in between. The repetitive injury was carried out for 7 and 15 days, in 2D- and 3D-TMs, respectively. At each check point time, cell metabolic activity was assessed by Alamar blue test in real time, revealing that cell-flattening of 2D-TM showed a different sensitivity to H_2O_2 chronic exposure compared to 3Ds. Indeed, during chronic oxidative stress, metabolic index resulted in a time-dependent increase in 3D-TMs, while did not vary in 2D culture. Furthermore, at the end of experimental treatments, cleaved PARP-1 was found in both static 2D- and 3D-TM, instead biodynamic 3D-TMs shown an increase of full-length PARP-1 only. To investigate the co-factor role of PARP-1 in inflammation pathway via NF-kB, the activation of this latter marker was analysed, under chronic oxidative stress [3]. Activation of the transcription factor was observed only in both 3D-TMs, but mostly in biodynamic models. Further analysis were performed to verify apoptosis in biodynamic 3D-TM, during the first 72 h exposure to chronic oxidative stress, by a dedicated protein array. The observed increase of several proapoptotic markers at 48 h only, would suggest a progressive cellular adaptation to pro-oxidant stimulus. Taken together these findings, dynamic 3D-TM showed features more closely to *in vivo* pathophysiology.

References

[1] Saccà, S. C. et al. (2016). *Ageing Res Rev 29*, 26-41.
[2] Izzotti, A. et al. (2015). *Mutat Res 772*, 1-9.
[3] Hassa, P. O. et al. (2002). *Cell Mol Life Sci 59*, 1534-1553.

Submission declaration:
Conflicts of interest: The corresponding author declares that there is no conflict of interest with the authors.
Statement on ethics vote: No ethics vote is required.